REVISTA MATÉRIA V.30
ISSN 1517-7076 articles e20250415, 2025

Design and analysis of a dual energy storage system with battery–supercapacitors integration for EV applications

Karthik Kambala[1], Ponnambalam Pathipooranam[1]

[1]Vellore Institute of Technology, School of Electrical Engineering. Vellore, Tamil Nadu, India.
e-mail: karthik.k2020@vitstudent.ac.in, ponnambalam.p@vit.ac.in

ABSTRACT

This paper introduces a sophisticated dual energy storage system (DESS) designed to enhance the efficiency and performance of electric vehicles. The system strategically combines a primary photovoltaic (PV) energy source with secondary battery and supercapacitor storage. Leveraging the rapid charge-discharge capabilities and high-power density of supercapacitors alongside the high energy density of batteries, the DESS aims to optimize power delivery by effectively balancing long-term energy storage with instantaneous power demands, particularly for regenerative braking and rapid acceleration. The operational strategy involves the supercapacitor handling high-frequency current fluctuations and the battery addressing low-frequency components, resulting in a smoother voltage profile compared to conventional systems. Optimal sizing and integration of these components are determined based on specific load requirements, voltage levels, energy capacity, and cycling life. The DESS, integrated with a permanent magnet synchronous motor (PMSM) in the d and q axes, undergoes rigorous testing under diverse real-world conditions, including varying wind and terrain, with and without braking. Simulations using MATLAB and DSPACE hardware 1KW PMSM to validate the system's current profile, voltage regulation, power split operation in different load conditions, and overall energy efficiency, demonstrating a significant improvement in the reliability, performance, and efficiency of electric vehicles. The proposed system achieves a DC-link voltage regulation of 48 V, improves energy efficiency by 12%, and extends battery lifetime by reducing stress currents by 18%.

Keywords: Photovoltaic; Battery; Supercapacitor; Bidirectional DC-DC converter; Permanent Magnet Synchronous Motor.

1. INTRODUCTION

Electric vehicles are currently being developed as an alternate method of transportation since the negative impact of internal combustion and environmental concerns is rising substantially. The National Oceanic and Atmospheric Administration (NOAA) releases global warming statistics yearly, showing 2023 as the sixth hottest year since 1880, per universal climate data [1]. However, there are environmental issues with electric vehicles. The biggest problem for every government is controlling air pollution, which causes respiratory diseases, cardiac problems, and lung cancer in 99% of humans, according to the World Health Organization (WHO) [2]. A DESS system combines the capability of both batteries and supercapacitors to create an efficient energy storage solution. Batteries offer high energy density but may have limitations in terms of fast charge and discharge rates; the Supercapacitor, on the other hand, provides high power density and fast charging/discharging capabilities but has lower energy density compared to batteries. By integrating these two technologies, a dual energy storage system can leverage the strength of each component. Batteries can handle long-term energy storage needs, while capacitors can handle sudden power demands and provide rapid bursts of energy [3].

The EV sector helps economic growth, and the country's various government schemes and motivations encourage consumers to switch to electric vehicles. China, the most populated country, ranks top in plug-in light-duty EV sales, which are supported. India, the world's second-most populous nation, is developing EV technology and producing several start-up business enterprises [4]. Although electric vehicle transportation began in 1827, it has been ineffective due to a lack of battery technologies. Researchers have developed several advancements in electric vehicles since the twentieth century, including energy storage devices and improved power electronic converters [5].

The Electrical Measurement process was carried out using a robust optimization approach. In this approach, the authors considered uncertainty in the cost function and compared their findings to those of other

Corresponding Author: Ponnambalam Pathipooranam Received on 11/05/2025 Accepted on 27/08/2025

DOI: https://doi.org/10.1590/1517-7076-RMAT-2025-0415

optimizing methods. This methodology's input sources include batteries, ultracapacitors, and fuel cells. However, there is no hardware implementation or operating cycle [6].

There have been proposals for hybrid energy storage systems that combine supercapacitors and Li-ion batteries. Supercapacitors can be a useful addition to Li-ion batteries by supplying peak power during transient events and enhancing energy recuperation efficiency. Their high-power density distinguishes them, as well as their quick charge/discharge capability and extended cycle life. In addition to improving EVs' dynamic performance, supercapacitors' integration with Li-ion batteries reduces battery stress and increases battery. Lifespan. Additionally, hybrid energy storage systems can raise EVs' overall energy efficiency, improving their dependability and sustainability.

Solar-powered BEVs should be designed with these basic hardware considerations in mind: The maximum power point tracking module uses the amount of diffused solar radiation to calculate the energy the panel can generate. Solar panel dimensions: This term typically describes the area of the vehicle that gets more sunlight during the day [7].

The solar panel size, the amount of sunlight, and the battery-charging cycle all significantly affect how long it takes for the battery to charge. This information helps the user choose the vehicle's operating mode. BMS and MPPT modules are, hence, essential parts of solar-powered BEVs. In addition to BEVs, the EVs of supercapacitors provide extra advantages to the controller recommended for the vehicle in this study.

By optimizing total performance, this system improves longevity, power delivery, and energy efficiency. Applications for dual-energy storage systems include grid stabilization, renewable energy systems, electric vehicles, and any situation requiring high energy and high-power density. Assume that the energy density and significant power of an electric vehicle. Then, because of the three-control performances of a permanent magnet synchronous machine and its work's rule-based and dynamic programming-based algorithm, it can operate for extended periods with rapid acceleration, giving the battery bank a longer time [8]. Because of the Supercapacitor and Battery, the system has to regulate the temperature. PMS functioning is achievable with the support of a thermal management system, as the authors showed by demonstrating an equivalent demand for the controller [9].

The following are fundamental hardware parameters to be considered for the implementation of solar-based Battery Electric Vehicles (BEVs):

(a) *Solar Panel Sizing*: Determined by the surface area of the vehicle that receives maximum solar irradiance during daylight hours, ensuring optimal energy harvesting.
(b) *Maximum Power Point Tracking (MPPT) Module*: Utilized to extract maximum power from the solar panel by dynamically adjusting operating conditions in response to varying levels of diffused solar irradiance.

A sizing method for batteries and supercapacitors (SCs) has been studied, and an integrated control strategy for power sharing between Hybrid Energy Storage Units (HESUs) has been developed using an adaptive approach. A computational experiment has been conducted using MATLAB and D-SPACE hardware to validate the system's current profile, voltage regulation, power flow management, and overall energy efficiency. The results demonstrate significant improvements in the reliability, performance, and efficiency of electric vehicles.

The proposed work uniquely combines renewable source integration, hybrid energy storage, Super Capacitor, MPPT, self-charging, vehicle dynamics, and a validated control strategy, making it a more holistic and novel solution compared to other studies.

Table 1 is a Summary of the literature review for the comparative analysis reveals that forecast-integrated optimization offers the most promising results in terms of cost, sustainability, and predictive accuracy. However, each study contributes uniquely to the field, whether through algorithmic innovation, system design, or energy management strategies.

This table serves as a valuable reference for selecting appropriate methodologies and optimization techniques based on specific objective be it cost reduction, fuel efficiency, or environmental impact.

2. SYSTEM DESCRIPTION

A hybrid electric vehicle (HEV) power flow control system architecture is depicted in block diagram form in Figure 1. The main elements of the block diagram are the PV Module, Boost Converter, Buck-Boost Converter, and the MPPT control. The PV module connects the mediator boost converter to a DC power source. In order to meet the requirement for a reduced load, PV electricity enters the DC connection and is either used by the load or stored in batteries. Supercapacitors inside and outside the batteries supply power to the load, while supercapacitors control the power from the batteries. The system utilises both supercapacitors and batteries, combining their complementary characteristics. Supercapacitors offer high power density and fast response, while batteries

Table 1: Summary of literature review.

REF	OBJECTIVE	METHODOLOGY	TECHNIQUE	PERFORMANCE	RESULTS AND OBSERVATIONS	LIMITATIONS
BARAKAT et al. [10] (Achieving Green Mobility)	Minimise TNPC and LPSP for PV-Wind-Battery EVCS	Bi-objective optimization; sensitivity analysis; HOMER validation	MOPSO, NSGA-II, NSGA-III, MOEA/D	NSGA-II best in convergence, diversity, robustness; NSGA-III most efficient	PV capacity: 223 kW; SOC: 60–96.6%; seasonal shift in energy sources; load variation most affects LPSP	Single-site case study; deterministic modelling; no V2G or dynamic pricing
ALSHAMMARI et al. [11] (Comprehensive Analysis of MOO)	Design a hybrid EVCS considering seasonal variations, TNPC, and LPSP	Comparative evaluation of 4 MOO algorithms: performance metrics analysis	MOPSO, NSGA-II, NSGA-III, MOEA/D	NSGA-II best overall; NSGA-III highest efficiency; MOEA/D most robust	TNPC: $564,846; LCOE: $0.2521/kWh; LPSP: 1.21%; NSGA-II most balanced	Focused on urban EVCS; limited real-time adaptability
SAMY et al. [12] (Decision-Making & Optimal Design)	Develop a decision-making model to select an optimal algorithm for a hybrid PV-Wind system	Statistical tests (ANOVA, Tukey); ANN modelling; performance comparison	PSO, HFAHS, Cultural Algorithm, Harmony Search, Simulated Annealing	PSO outperformed others in statistical and ANN-based evaluations	TNPC: $3.88M; LCOE: $0.22/kWh; LPSP most influential factor; ANN R2 = 99.7%	Case-specific to Ras Sedr, Egypt; only five algorithms tested; the ANN model needs broader validation
GÜVEN et al. [13] (Design Optimization of Standalone System)	Minimise ACS and LCOE for university campus HRES	Rule-based EMS; MATLAB simulation; HOMER comparison	Harmony Search, JAYA, Ant Colony Optimization	HS fastest convergence; lowest ACS and LCOE; JAYA better than ACO	HS: ACS = $400,840; LCOE = $0.2012; REF = 100%; PV = 2608 kW; Batt = 1996 units	Focused on one site, deterministic modelling, no stochastic analysis
SAMY et al. [14] (Exploring Energy Storage for Grid Outages)	Compare battery technologies under grid outage scenarios	HOMER simulation; techno-economic analysis; grid failure modelling	HOMER with LA, LI, VR, NI, ZB batteries	LI battery best for moderate outages; VF and NI better for high outages	COE: $0.085–$0.099/kWh; REF: 30–33%; IRR up to 30%; SPB as low as 3.5 years	Limited to one school site; no dynamic pricing or V2G; fixed load profile
ZEREG and BOUZGOU [15] (Forecast-Integrated Optimisation in Hyper-Arid Regions)	Minimise LCOE and LPSP; maximise RF using forecast-driven HRES	ML/DL forecasting + MOPSO optimisation; HOMER validation	BiLSTM, Random Forest, CNN-LSTM + MOPSO	LCOE = $0.054/kWh; LPSP = 3.1%; RF = 98%; 80% CO2 reduction vs diesel-only	PV = 47%; Batt = 35%; Wind = 12%; Diesel = 6%; NPC = $21,357	Forecasting errors affect sizing; single-site case; battery emissions are high
ABDELDJALIL et al. [16] (FC-HEV Sizing and EMS)	Integrate optimal sizing and EMS for fuel cell hybrid EVs	MOPSO-based MATLAB optimisation; tested under ARTEMIS and NEDC cycles	Multi-objective PSO; EMS with battery + supercapacitor	Battery + SC reduced fuel consumption by 19–30%; FC max power reduced by 6–19%	Operating cost reduced; fuel consumption minimised; improved performance under dynamic loads	Limited to simulation; no real-world deployment; focused on FC-HEV only
SAMY et al. [17] (Flower Pollination Optimisation for PV-FC System)	Minimise TNPV and LPSP for off-grid PV-FC hybrid system	Techno-economic modelling; MATLAB simulation; sensitivity analysis	Flower Pollination Algorithm (FPA), compared with ABC, PSO	FPA fastest convergence; lowest TNPV and LCOE	Optimal config: 27 PV, 28 FC, 58 electrolysers, 37 H2 tanks; LCOE = $0.334/kWh	High FC cost dominates TNPV; limited scalability; single-site case
DJOUAHI et al. [18] (Thermal Control in FC-HEV)	Optimise sizing and thermal control of FC-HEV components	MOPSO-based MATLAB simulation; thermal controller integration	Multi-objective PSO with thermal modelling	The thermal controller reduced fuel consumption by 3.47%; improved FC efficiency.	FC temp control at 90°C improved performance; Li-ion + Maxwell SC best combo	Limited to Artemis cycle; no real-world validation; thermal effects not generalized
DJOUAHI et al. [19] (Optimal Sizing of Battery and SC)	Select the best battery-SC combo for FC-HEV under SFTP-SC03 cycle	MOPSO-based MATLAB simulation; multi-objective optimisation	Multi-objective PSO; comparative analysis of battery-SC types	Li-ion + Maxwell SC reduced fuel consumption by 0.43%, the lowest operating cost	SFTP-SC03 showed the lowest fuel use; Maxwell SC improved FC load sharing	Focused on one drive cycle; cost assumptions static; no real-time EMS
ETEIBA et al. [20] (Optimisation of PV-Biomass Hybrid System)	Minimise NPC and LPSP for off-grid PV-Biomass system	Comparative optimisation using 4 metaheuristics; HOMER validation	FPA, HS, ABC, FA	FA fastest convergence; lowest NPC; best performance	Optimal config: 24 PV, 4 biomass, 298 Ni-Fe batteries; LCOE = $0.084/kWh	Case-specific to Egypt; biomass assumptions fixed; limited battery types

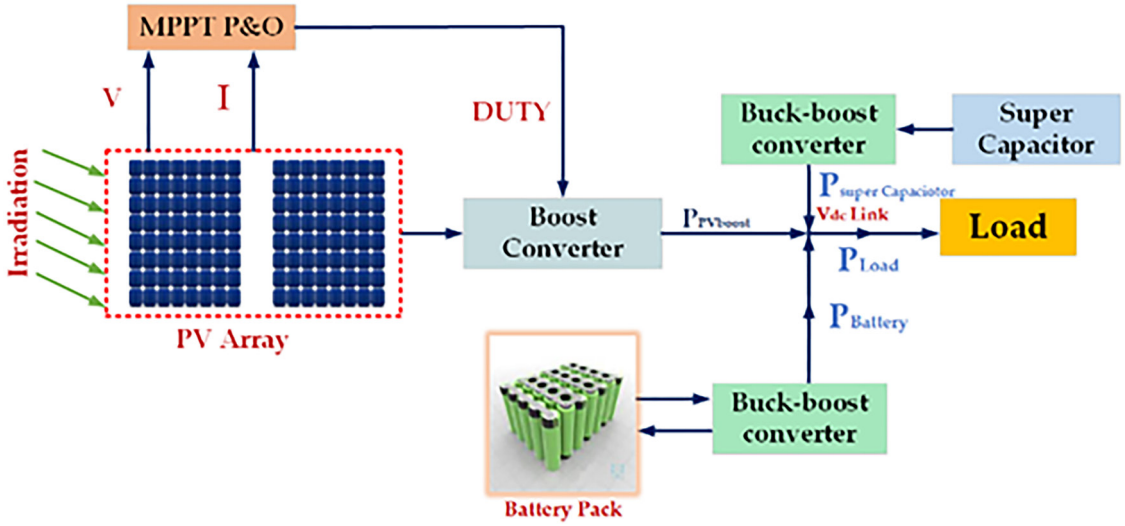

Figure 1: Block diagram for system configuration [21].

provide high energy density and long-term storage. The hybrid storage system improves the stability and reliability of the overall system by smoothing out power fluctuations and providing backup power. MPPT ensures that the maximum power is extracted from the PV array, maximizing the system's efficiency. The system can be adapted to various applications and load profiles due to its modular design and the flexibility offered by the hybrid storage system.

3. NUMERICAL MODEL OF AN MPPT WITH SOLAR PV PANEL

The mathematical models for PV arrays are based on the theoretical equations that describe the functioning of the PV cells and can be developed using the equivalent circuit of the PV cells. The empirical models rely on different values extracted from the characteristic equation of the solar panels using an analytical function. Many photovoltaic cell models have been developed in the literature to describe the behaviour of a PV cell. The most frequently used model is the traditional single-diode model, also known as the five-parameter model. Solar cells, machines that turn sunlight into electricity, are depicted in Figure 2. Understanding the performance of these devices, improving their design, and forecasting how they will behave in different scenarios depend on modelling them. Modelling strategies for the physical, empirical, and equivalent circuit models. A numerical model of an MPPT (Maximum Power Point Tracking) system with a solar PV panel involves simulating the behaviour of the PV panel, the MPPT algorithm, and the load.

$$I_L = I_{ph} - I_d - I_{Sh} \tag{1}$$

$$I_d = I_{Rd}[Exp\left(\frac{V_L + I_L R_S}{n.V_t}\right) - 1]n \tag{2}$$

$$V_t = \frac{K.T}{q}$$

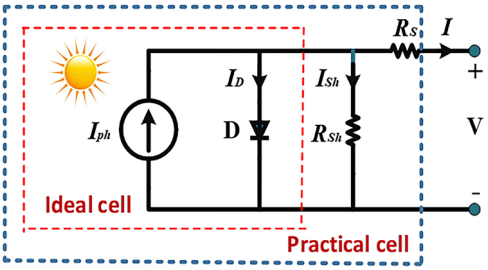

Figure 2: Model of a solar cell.

$$I_{pv} = I_{ph} - I_{Rd}\left[exp\left(\frac{V_L + I_L R_s}{n.V_t}\right) - 1\right]\frac{V_L + I_L R_s}{R_{sh}} \tag{3}$$

$$I_{ph} = \left[I_{Sc} - STC + K_s(T - T_{STC}) - \left(\frac{G}{\cdot G_{STC}}\right)\right] \tag{4}$$

$$I_{Sh} = \frac{V_L + I_L R_s}{R_{sh}}$$

In the single-diode model, the current source is used to model the incident solar irradiance, a diode for the polarization phenomena, a series resistance and a parallel resistance to represent the power losses. Using Kirchhoff's law, the cell terminal current is the most commonly used model. It represents the PV cell as a current source, a diode, a series resistance (Rs), and a parallel resistance (Rp).

Where Iph and Io are the photo-generated current and the dark saturation current of the PV system, respectively, and Vt = Ns kT/q is the thermal voltage of the PV system with Ns cells connected in series, Rs and Rsh are the cell series resistance and the cell shunt resistance, respectively, a is the diode quality factor, q is the electronic charge 1.6 × 10−19C, k is the Boltzmann's constant 1.38 × 10−23 J/K, and T is the ambient temperature, in Kelvin. The short circuit current (SCC) under standard test conditions (STC) is abbreviated as the Isc short circuit current coefficient, established as Ks GSTC. The irradiance and temperature values at the STC are 25 °C and 1000W/m^2, respectively [22]. Where I_{ph}, I_D, I_{RD} and R_{sh} E represents the photo-generated current, diode current, reverse saturation diode current, and shunt resistor current, respectively. The identity factor of the diode is represented by n, and the series resistance is described with R_s and V_t Represents the junction thermal voltage. The Boltzmann constant, defined as k, is 1.3806503 × 10^{23} J/K. The electron charge, q, equals 1.60217646 × 10^{19} C, and the temperature, T, is expressed in Kelvin. The I_L and V_L The output voltage and current, respectively represent the calculated data that the manufacturer has earlier determined, as well as the values of q, k, and T. Consequently, there are five unknown parameters. (I_{ph}, I_{RD}, n, R_s, and R_{sh}) Calculated and enhanced parameters are required. Determining the parameters is difficult since they significantly affect the efficiency and reliability of the solar cell.

$$P_{pv} = v_{ph} - N_{pl}\left[I_{ph} - I_0 Exp\left(\frac{qV_{pv}}{N \cdot scTAK}\right) - \left(\frac{V_{pv}}{\cdot N_{sc}}\right)\right] \tag{5}$$

The solar PV system operates at maximum power point (MPP), as seen in Figure 3, and its ability to raise the MPP position for an extended period is not sustained. Equation models can be used to carry it out, though. Because of its incremental resistance, the MPPT methodology offers a variety of better adaptable methods because of its rapid response, value, and application to real-world situations [23].

$$d(m) = \left[d(m-1) - \pm s\left|\frac{dP}{dV}\right|\right] \tag{6}$$

$$d(m) = \left[d(m-1) - \pm s\left|\frac{P(m) - p(m-1)}{v(m) - V(m-1)}\right|\right] \tag{7}$$

The duty ratio of the boost converter is called the S from the above two equations, and d(m) identifies the scaling factor to maintain the step size in an investigation. The VSS-INR algorithms determine MPPT accuracy for optimal MPPT operation. The following rule solves the following equation.

$$\mathrm{d(m)} = \left|\frac{dP}{dV}\right| \leq \Delta dmax \tag{8}$$

The above equation is the higher step size and high level for the number of steps and the scaling factor.

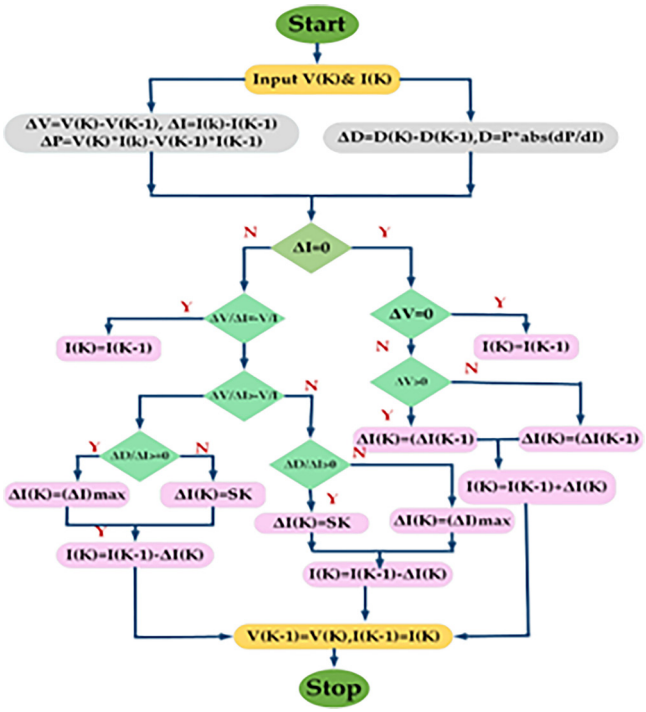

Figure 3: Flow chart for solar MPPT.

$$S \leq \Delta dmax / \left|\frac{dP}{dV}\right| \tag{9}$$

S: scaling factor

The methods used in MPPT can be altered to specific ranges in the threshold values. The valid range of the photovoltaic cell's power derivative [dP/dI], as well as the exponential values of PV. Output power P_{ex} is the slope between Power and current is known to be [dP/dI], which is defined in the paragraph that follows

$$B = Pex\ X \left|\frac{dP}{dV}\right| \tag{10}$$

$$\left|\frac{dP}{dV}\right| = |tan\Phi| \tag{11}$$

The above equation's limit is between -90º & 90º°.

The duty cycle continually regulates this MPPT system's boost converter to obtain the maximum power point, utilizing a variable step size method. By modifying the duty cycle, the solar panels' reference current, known as Iref, can be obtained when solar PV performs. When maximum Power is reached, I_{ref} = IMPP, and ΔIref) The maximum is set by the standard in adjustable step size mode.

$$V_{SK} = (\Delta Iref)\, maximum \times sin\Phi k \tag{12}$$

In the above equation, VSk represents the variable step size at a specific period k. Since k starts from 0 and goes up, VSk signifies the step size at different points in time. Sin (Φk) This term likely represents the oscillation of some variable, possibly the voltage or current, at period k. Φ (phi) is a standard notation for the phase angle in electrical engineering.

The exact relationship between VSk, sin(Φk), and the duty cycle oscillation would depend on the specific system and control algorithm [24]. The given information does not clarify the impact of VSS-INR on the duty

ratio size. More context about VSS-INR and its connection to the duty cycle would be needed for a complete understanding.

4. ENERGY STORAGE SYSTEM

Energy Storage Systems (ESS) can store available energy from renewable energy and be used during peak hours of the day. Figure 4 shows Energy storage systems classified based on the type of energy they store and the technology. These electrochemical energy storage devices are lead-acid, lithium-ion, and nickel-metal hydride batteries. Flow batteries store energy in electrolytes, allowing for flexible scaling and longer life.

As per the National Electricity Plan (NEP) 2023 of the Central Electricity Authority (CEA), the energy storage capacity requirement is projected to be 82.37 GWh (47.65 GWh from PSP and 34.72 GWh from BESS) in the years 2026-27. This requirement will increase to 411.4 GWh (175.18 GWh from PSP and 236.22 GWh from BESS) in 2031-32. Further, CEA has also projected that by the year 2047, the requirement of energy storage is expected to increase to 2380 GWh (540 GWh from PSP and 1840 GWh from BESS) due to the addition of a more significant amount of renewable energy in light of the net-zero emissions targets set for 2070 [25]. The Ministry of Power has also notified a long-term trajectory for Energy Storage Obligations (ESO) to ensure sufficient storage capacity is available with obligated entities. As per the trajectory, the ESO shall gradually increase from 1% in FY 2023-24 to 4% by FY 2029-30, with an annual increase of 0.5%. This obligation shall be fulfilled only when at least 85% of the total energy stored is procured from Renewable Energy sources annually.

4.1. Battery

Batteries are electrochemical devices that store and release electrical energy. They are classified based on their chemistry, construction, and intended use. Figure 5 represents batteries and electrochemical devices that convert stored chemical energy into electrical energy. They come in various forms, each with its characteristics and applications. There are two types of batteries: primary batteries and secondary batteries. The best battery type for a particular application depends on factors such as Energy density, Power density, Life Span, safety, and cost.

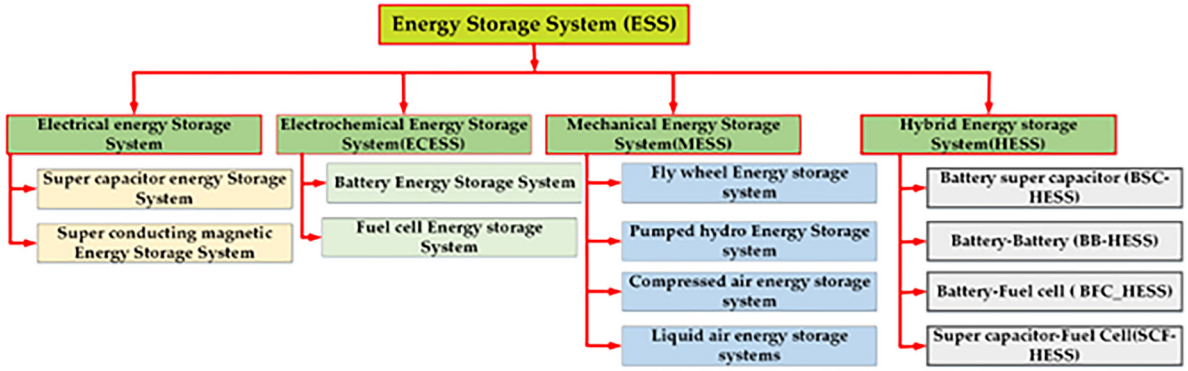

Figure 4: Classifications of energy storage systems.

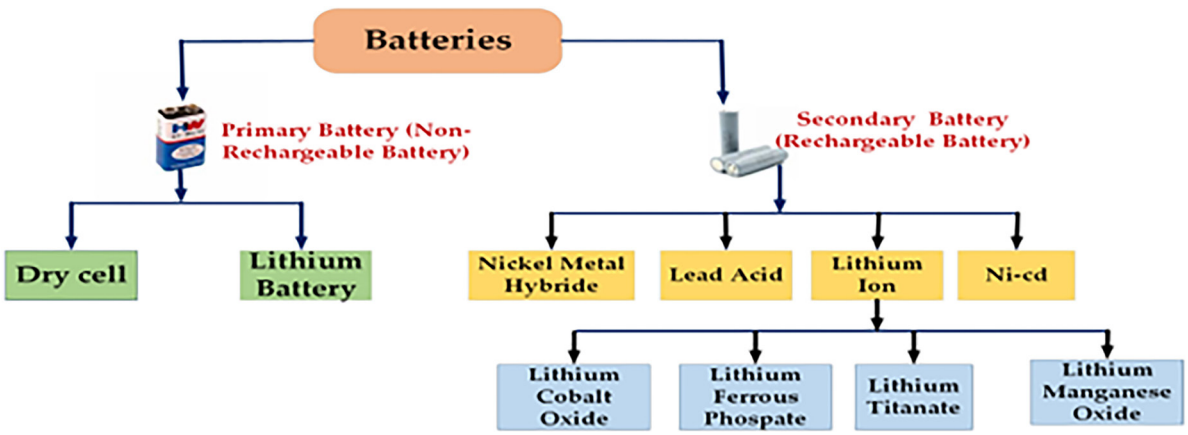

Figure 5: Types of batteries.

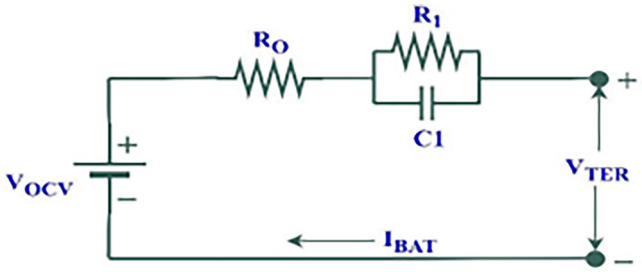

Figure 6: Battery cell model.

EV batteries rely on materials like lithium, nickel, and cobalt, raising concerns about their environmental and social costs during mining. The extraction of these materials can harm the environment, causing soil erosion, water contamination, and habitat loss. The projected 40-fold increase in lithium demand by 2050 (as estimated by the World Economic Forum) highlights potential resource limitations. The true environmental benefits of electric vehicles depend on their power source. If charged primarily by electricity generated from fossil fuels, they may not significantly reduce pollution compared to internal combustion engines. Widespread adoption of renewable energy sources and integration of energy storage systems are crucial for achieving significant decarbonization. Furthermore, energy storage systems should be emphasized, particularly in the transition towards a carbon-free future, as it's vital for effectively integrating and utilizing the intermittent power generated from renewable energy sources like wind and solar.

Moreover, the products emit many greenhouse gases, such as carbon dioxide. The Battery is the principal energy source in this EV System, and it can power the PMSM load if the Supercapacitor and solar fail to deliver Power. Choosing the correct battery is critical in EVs in terms of mileage, battery cells, and modules. C- rate of charge, depth of discharge [26] (Figure 6).

$$V_{TER}(t) = V_{OCV}(SOC(t)) - R_o I_{BAT}(t) - V_1(t) \tag{13}$$

The diagram shows that the battery cell model is C, R1 is the parallel resistance and Capacitance, and V_{TER} and I_{BAT} are the terminal voltage and current delivered by the battery cell. The battery power employed in this simulation is 81 kWh, with an initial voltage of 540 V [27]. A single battery has 12V and 150 Ah capacity, whereas 40 batteries paired in series provide 480V and 150 Ah capacity. To determine the SoC range, battery Life, and Safety, overcharging a Battery beyond its capacity can lead to internal damage, such as the formation of dendrites (Metallic growth) that can cause short circuits and even explosions. The over-discharging and draining of a battery completely can permanently damage the internal chemistry, reducing its lifespan and capacity. An accurate SoC for thermal management is essential. Excessive charging/discharging can generate heat, potentially leading to thermal runaway and safety hazards. Battery cycling frequency between 0% and 100% SoC can significantly shorten battery lifespan and reduce stress. The battery's reduced stress operation is within 20% & 80%. The range minimises stress on the battery, leading to a longer lifespan and better performance. Improved safety in the range avoids the risks associated with deep discharge and overcharging. Operating within a recommended range, such as 20% to 80% [28].

The bidirectional power modulator charges and drains the Battery according to the SoC level. The charge and discharge quadratic boost converter maintains a constant voltage of 434V via the Battery's charge and discharge switch while the controller modifies the duty cycle frequency [29] (Figure 7).

Battery Energy Storage Systems (BESS) are crucial components in photovoltaic (PV) systems, especially in regions with fluctuating solar irradiance or high energy demand during peak hours. They store excess energy generated by the PV system during sunny periods for later use when solar generation or demand is low.

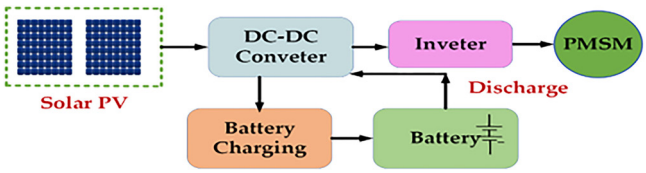

Figure 7: Battery energy storage system for PV system.

Represents the energy storage system, which is the set of methods and technologies used to store various forms of energy [30]. The battery energy storage system (BESS) for Systems is a DC/DC converter that provides DC link voltage to the inverter from the Battery. When selecting a BESS for system size, battery chemistry, Depth of Discharge (DOD), Cycle Life, and Efficiency are the factors to consider.

4.1.1. During the charging process

Any liquid or solid substance that permits ions to flow through it is called an electrolyte, and it facilitates this movement. Nickel manganese cobalt oxide (NMC) or lithium cobalt oxide are layered oxide materials that make up the cathode. Figure 8 shows an anode composed of silicon or graphite. Electrons flow from the external charger to the anode to create a positive and negative charge as lithium ions migrate from the cathode to the anode. The two electrodes develop a potential difference as a result, which propels the lithium ions to migrate. The BMS tracks temperature, voltage, current, and state of charge. Charging and discharging procedures are also regulated to guarantee optimum performance and security [31]. The Charging system supplies electrical energy to the Battery during Charging. The Load draws electrical energy from the Battery during discharging. The Power electronics control the flow of electrical energy between the Battery, charger, and Load. This can include components like DC-DC converters, inverters, and rectifiers.

4.1.2. During the discharging process

Figure 9 shows the opposite Process during discharging. To create electrical energy, electrons move from the anode to the external circuit, and lithium ions return to the cathode. After receiving electrons and lithium ions,

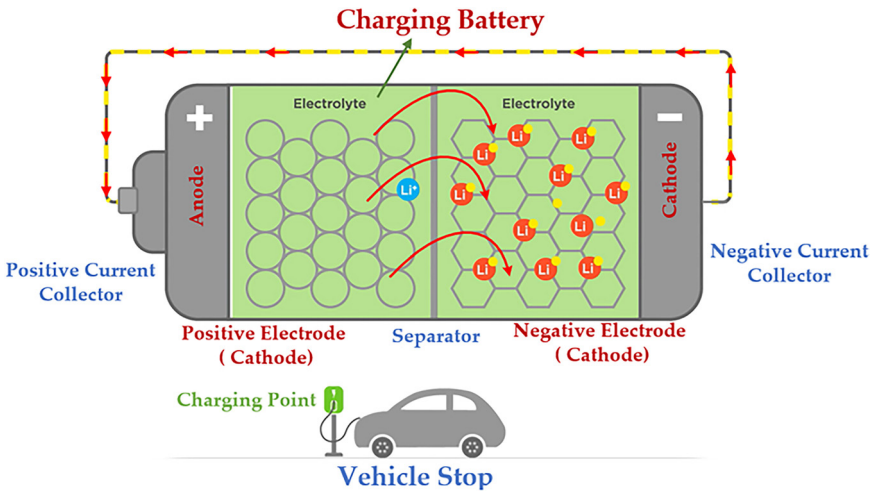

Figure 8: The lithium-ion battery is charging.

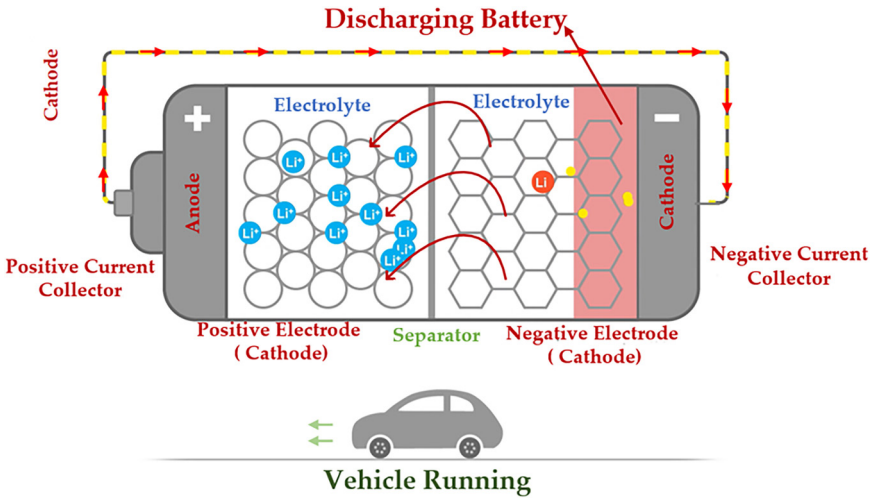

Figure 9: The lithium-ion battery is discharging.

the cathode acquires a negative charge. Lithium ions and electrons leave the anode and become positively charged [32].

4.2. Super capacitor or ultra capacitor

Supercapacitors, sometimes referred to as ultracapacitors or electric chemical capacitors, are energy storage devices that use the electrostatic separation of charges to store electrical energy. Supercapacitors have a high cycle life and can charge and discharge quickly because they store energy electrostatically rather than chemically, as conventional batteries do. With densities so high that they are commonly utilized in battery applications, supercapacitors provide the highest capacitive density of any capacitor currently available. The recommended option in applications necessitates storing significant energy and delivering it regularly [33].

The equivalent circuit, a simplified or first-order model of an exceptional capacitor, is shown in Figure 10. Since the electrodes are made of porous materials, real supercapacitors have more lines than capacitors. The capacitor's circuit may be shown more accurately. Various methods can be used to measure Capacitance.

- Method of Charging
- Method of charging and discharging: The charge method calculates the measurement and formula [34].

The charging and discharging mechanism, which involves storing and releasing electric energy in a capacitor, is depicted in Figure 11. A voltage source is linked across the capacitor during charging, progressively raising the voltage. When a capacitor is discharged, the electrical energy that has been stored is released. The capacitor begins to discharge when it is connected to a circuit with a voltage lower than its charged voltage. As time passes, the Output's current and the voltage across the capacitor drops [35]. A capacitor's charging and discharging follow exponential curves, and the time it takes to charge and discharge significantly depends on the capacitator and the resistance in the circuit. The equations governing these processes are based on the R.C. time constant.

$$t = \left(\frac{C_x (V_0 - V_1)}{t} \right) \tag{14}$$

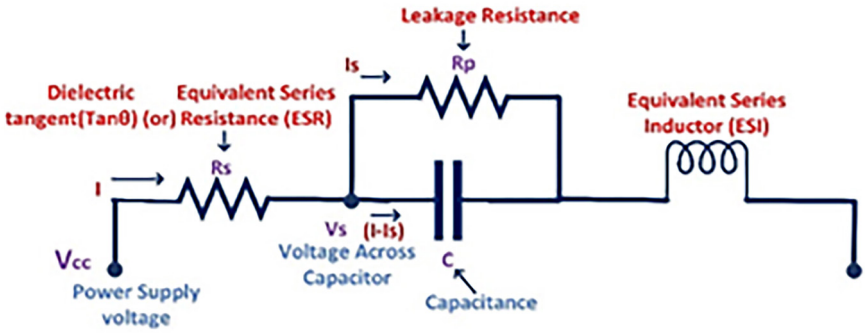

Figure 10: Supercapacitor for equivalent circuit.

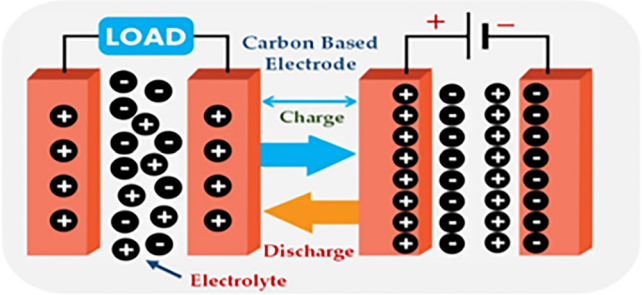

Figure 11: Charging and discharge method for ultra super capacitor.

Where R = resistance

C = Capacitance in the circuit.

Constant Current Discharge time

For Constant resistance discharge

The time is determined by

$$\left[t = C * \left(Rin \frac{(V_1)}{(V_0)} \right) \right] \tag{15}$$

4.3. Permanent Magnet Synchronous Machine (PMSM)

In the motor mathematical model, the d and q axes in a PMSM represent the two orthogonal axes. As seen in Figure 12, the q-axis is perpendicular to the d-axis, which is aligned with the rotor magnetic fields. Vector control approaches use the axis to make controlling the motor easier [36]. When the three-phase AC system is converted to a two-axis system (d-q axis), the motor's torque and flux can be more easily controlled individually.

$$V_{di} = \text{Rstidi} + \frac{d\lambda di}{dt} - \omega re\lambda qr \tag{16}$$

$$\text{Vqi} = \text{Rstidi} + \frac{d\lambda di}{dt} - \omega re\lambda di \tag{17}$$

From the above Equation

Vdi and Vqr = Direct axis voltage and quadratic axis voltage

Idi and Iqr = Direct axis current and quadrature axis current (A)

λdi and λqr = flux linkage in the stator of the direct and quadrature axis (Wb)

ω_{re} = angular velocity of the rotor

Rst = stator resistance

The flux linkage of the stator equations is

$$\lambda di = \text{Ldi} + \lambda ro \tag{18}$$

$$\lambda qr = \text{Lqriqr} \tag{19}$$

The stator inductance from the direct-quadratic axis is Ldi & Lqr (H),

λro = flux linkage of the rotor at the normal time (Wb).

The electromagnetic torque generation can be represented as:

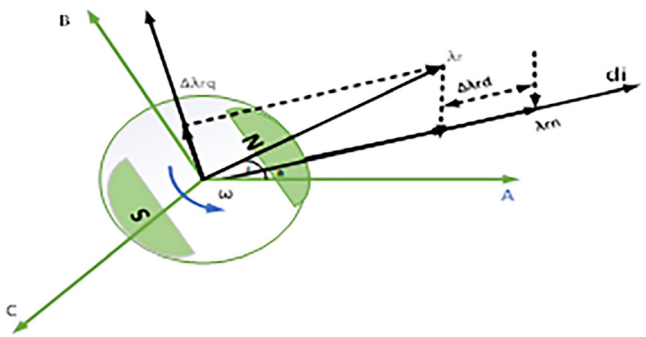

Figure 12: Flux linkage system.

$$\text{Tel} = \frac{3}{2}\text{nPol}\ \lambda\text{diiqr} - \lambda\text{qridi}$$

$$= \frac{3}{2}\text{nPol}\ \lambda\text{ro} + \text{Ldi} - \text{Lqr idi. iqr}$$

$$\text{Tel} = \frac{3}{2}\text{nPol}\ \lambda\text{ext iqr} \tag{20}$$

Where Tel = Mechanical angular Velocity (rad/s)

V = viscous coefficient, J is the moment of inertia (Kg.m^2)

$$\frac{d\omega_{re}}{dt} = \frac{n_{pol}}{J}(T_{el} - T_1 - V\omega_M) \tag{21}$$

Where ω_M = mechanical angular velocity(rad/s), T1 = load torque(N-M)

5. VEHICLE DYNAMIC MODELLING

5.1. Vehicle modes of operation

5.1.1. Vehicle normal mode

When the Battery's rated Power exceeds the motor's necessary Power in Normal Mode, the Supercapacitor does not give the motor power. Hence, the Battery supplies the motor [37]. During the day, the Solar PV array charges the Battery, which is used for regular motor acceleration. This guarantees a renewable mode of operation.

Cruising is the Process of keeping a constant speed with little fluctuation. It is frequently used for automobiles, motorcycles, or electric vehicles. Figure 13 illustrates the cruising required to keep speed steady while maximizing energy use in an EV. Corresponding to a motor [38]. This can be achieved through efficient motor control algorithms, proper power management, and aerodynamic considerations for the driving experience while maximizing the vehicle range by minimizing energy losses.

5.1.2. Vehicle traction mode

The vehicle switches to traction mode when the battery cannot meet its needs. Since the battery pack is the main energy source in this example and provides power to the motor when fully charged, the Supercapacitor helps the battery by providing extra power to the electric motor when needed. The Supercapacitor delivers the additional power required to run the motor if the power demand surpasses the battery pack's capacity. This makes it possible for the cars to operate more effectively and perform better, particularly while accelerating and when there are sudden spikes in power demands when driving. Upward, the power produced by the PV module will be used to charge the Supercapacitor, which the motor will then use when a strong torque is required to overcome the gradient force [39].

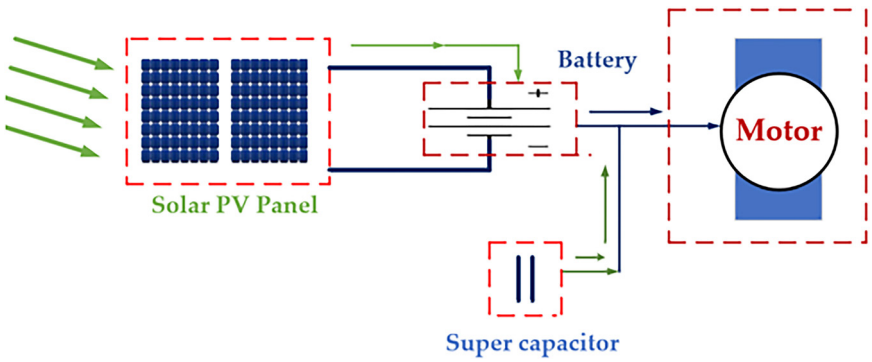

Figure 13: Cruising.

5.1.3. Climbing/acceleration mode

Climbing and acceleration are two essential aspects of a motor's Performance, especially in electric vehicles (EVs) equipped with motors like PMSM.

5.1.3.1. Climbing

When an electric vehicle needs to climb a hill or an incline, it requires more torque from the motor to overcome the gravitational force pulling it back. In this scenario, the motor must deliver a higher Torque to ensure the Vehicle can maintain an appropriate climbing speed. The motor control system must adjust the torque output based on the incline severity, vehicle weight, and other factors.

5.1.3.2. Acceleration

Acceleration refers to the rate at which the Vehicle increases its Speed to overcome friction and inertia; the motor must deliver a high Torque for swift acceleration. In EVs, instantaneous torque delivery is a significant advantage of electric motors as they can provide maximum torque even from a standstill. Efficient motor control algorithms are crucial to managing the torque output during acceleration while maintaining stability and avoiding issues like wheel slip [40].

The climbing and acceleration scenarios depicted in Figure 14 require sophisticated control strategies to regulate torque, current, voltage, and power delivery to the motor's sophisticated control systems. For instance, field-oriented control is frequently employed to maximize motor performance in various operating scenarios.

5.1.3.3. Breaking with super capacitor

When the brake is applied, regenerated Power enters the Supercapacitor. This reduces the number of charging cycles for the primary Battery, extending its life over time. Supercapacitors are high-energy-density capacitors capable of quickly storing and delivering large amounts of Power [41]. Their capacity to manage quick charging and discharging cycles makes them perfect for applications needing quick, high-power energy storage and delivery. Using supercapacitors for breaking has several benefits, including high power density, long cycle life, fast charging and discharging, and environmental friendliness. Despite price reductions, supercapacitors are still more costly than alternative energy storage solutions.

5.1.3.4. Single battery braking

Single-battery braking is a regenerative braking system where a single battery stores the energy recovered during braking. This approach is commonly found in electric vehicles (EVs) and hybrid electric vehicles (HEVs) [42]. When the Supercapacitor is ultimately charged, it will be open-circuited, and the Battery will take in any extra electrical energy generated during the regenerative braking process, provided that it has not been overcharged. In some cases, EVs and HEVs may use a combination of a battery and a supercapacitor for braking. Improved peak power handling, faster Charging and discharge, and Extended Battery Life.

5.1.4. Vehicle dynamic modelling

The proposed work uses ambulances, and the chapter examines the dynamic equations that control vehicle movements. The internal combustion engine-powered vehicle has numerous issues, including a high floor base that makes driving unsteady, limited acceleration with j, and strong vibration for the patient and the medical

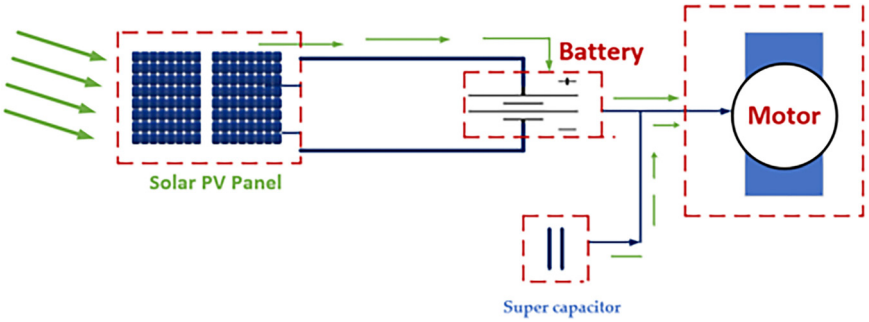

Figure 14: Climbing and acceleration.

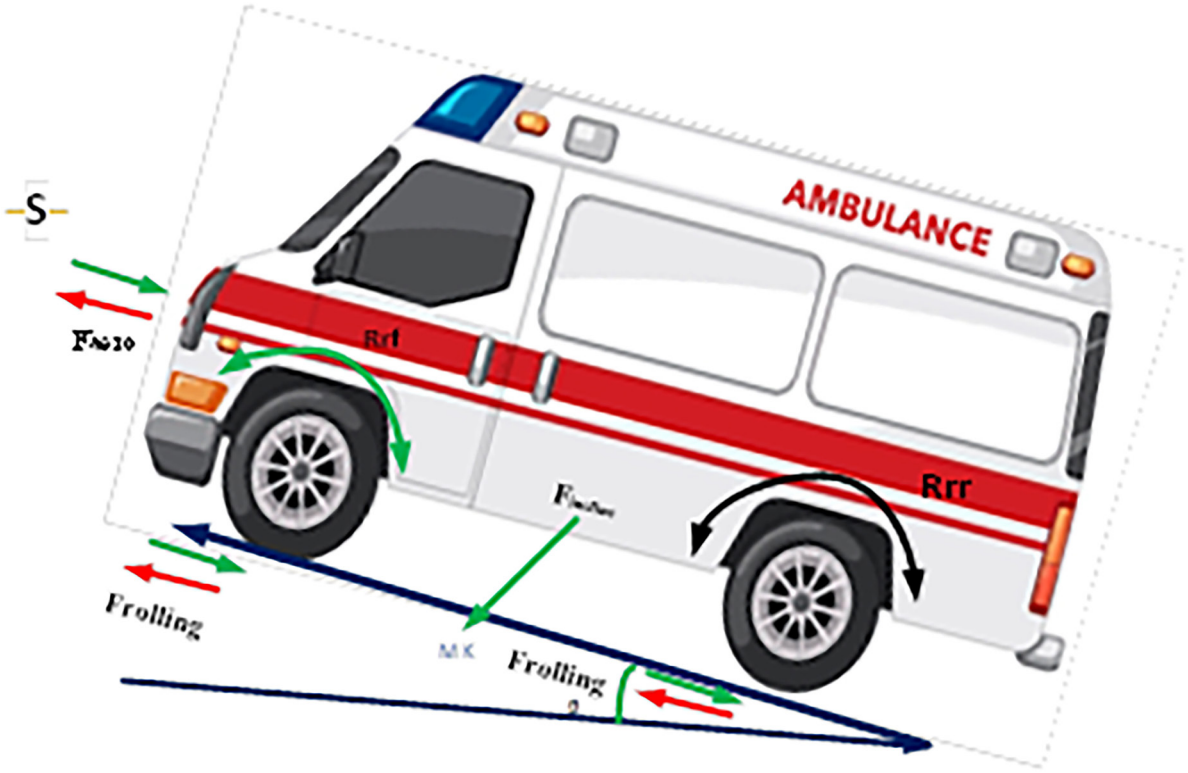

Figure 15: Vehicle dynamics for ambulance.

Table 2: Weight calculation for the proposed Ambulance vehicle.

Weight of the fuel tank and engine	750 kg
Kerb without engine/fuel tank	3350
Passenger weight and equipment weight	1000 kg
Fuel tank	56 kg
Hydrogen tank	100 kg
10 solar panels and Battery	406 kg
Motor	140 kg
Other weights	50 kg
Total	5000 kg

staff's treatment. In vehicle dynamics design, the workstation size is constrained so that the medical vehicle can be electric. Figure 15 explains the force acting on the car.

There are three different forces: Rolling opposition force, aerodynamic pull force, and Inclined resistance force. Newton determined that the ambulance bus's entire mass, gravity, and tyres exert the rolling opposing force [43].

$$Rr = mkd \tag{22}$$

Where Rr is the rolling opposition in force in Newton,

m is the mass of the vehicle in kg, and

K is the acceleration of gravity in m/s^2

The tyre deformation is measured in meters, and S is the bus's speed in meters per second. The total vehicle weight is distributed across various subsystems including the engine, fuel tank, hydrogen storage, solar panels, and passenger load, as detailed in Table 2.

The bus speed is expressed in meters per second, the tyre deformation in millimeters, and the S.M. is the maximum Speed of the bus (912 km/hr.), $P_{rolling}$= power of rolling opposite in watts

$$\text{Rolling} = 490.5 \times 90\ [1000/3600] = 12262\text{W}$$

$$R_{olling} = \mathbf{12.5W}$$

When a vehicle moves dynamically, the force impacts its forward movement and acceleration. The aerodynamic force generated by the Vehicle is given in the next equation [44].

$$F_{aero} = \left[\frac{1}{2}\rho \text{A frontal } S_2 \times S\right] \tag{23}$$

ρ = air density(1.23kg/m^2)

$A_{frontal}$= frontal area of the bus (6m^2)

ρ = air density(1.23kg/m^2)

From the above equation

$$\text{Fareo} = 1/2 \times 1.23 \times 6 \times 0.5 \times 252 \times 25 = 28828\text{W}$$

$$F_{aero} = \mathbf{29KW}$$

The Vehicle is any sloping road whose weight generates a force that forces it downhill at a 45^0 angle, integrating the resistive force formula.

$$F_{incline} = m\ k\ sin(\delta) \tag{24}$$

k is the angle of the road

$$F_{incline} = 5000 \times 9.80 \times \sin(45^{\circ})$$

$$F_{incline} = 34677\ \text{W}$$

$$F_{incline} = \mathbf{33\ kW}$$

The sum of all the forces acting on a vehicle is called the total force, as shown in the Equation.

$$F_{total} = F_{rolling} + F_{incline} + F_{aero} \tag{25}$$

$$F_{total} = 12\ \text{kW} + 29\ \text{kW} + 3\ \text{kW}$$

$$F_{Total} = \mathbf{76.3\ kW}$$

The Vehicle's Acceleration is measured by the second law of Newton, which states that each movement of the body depends on the total force exerted by the body. Vehicle movement forward position forces must outweigh opposing forces such as Wind, gravity, road, and tyre resistance. When converting an Intensive Care IC)- based ambulance to an EV ambulance, the PMSM is chosen based on its 76.3 kW [45].

6. SIMULATION AND RESULTS FOR VEHICLE DYNAMICS

The simulation results for the electric Vehicle's Vehicle modeling include additional features, such as a vehicle body and tired model, Wind and Terrain Effects, and a brake model. Sensor measurements are also used in this mechanism. Here, I have taken a half-car model for the prototype. The Vehicle is in zero condition. The constant value is positive i, e 100 [46].

Figure 16 shows three conditions: a zero condition, an upward condition, and a downward condition. When in the zero condition, the vehicle's speed is zero. Vehicle speed is positive while traveling forward and downward, and negative when travelling uphill.

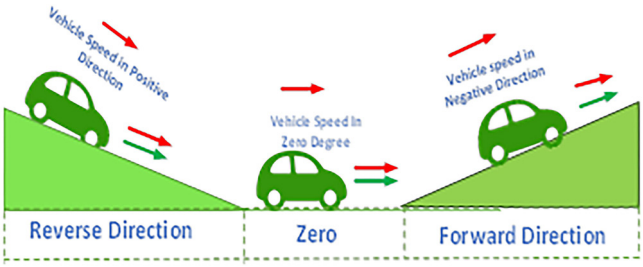

Figure 16: Vehicle in different conditions.

The three circumstances' waveforms are shown in Figure 17. The first condition is 0 rad, which denotes a zero-vehicle speed. 10*(π/180) is the second condition degree of the slope, indicating that the vehicle speed is in the opposite, hostile direction. The third criterion suggests that the vehicle speed is in the opposite and positive direction, which is -10*(π/180) [47].

Figure 18 represent the diagram illustrates car aerodynamics by showing how airflow interacts with the vehicle's shape. Black streamlines represent wind flowing from left to right, curving smoothly over the car's roof and sides. The airflow pattern highlights drag, lift, and turbulence zones, which influence fuel efficiency and vehicle stability.

Terrain and wind are two interrelated elements that majorly impact various activities, from cycling and hiking to building and transportation, as shown in Figure 19. Let's examine each of their traits in more detail and how speed and distance interact. Since slop will never change, the speed will remain constant after it reaches its maximum. Speed varies in tandem with changes in slope. Moreover, the converted distance continues to expand. The slope needs to have separate values for a data sheet to be generated for a certain period. What can the car do to determine whether the slope is zero [48]. Figure 20 represents Speed as a measure of how quickly an object moves, while distance is the length of the path travelled. These two factors can significantly influence the overall Speed and distance covered in the context of Terrain and Wind. Speed and distance covered in a given terrain can be substantially influenced by the characteristics of the Terrain itself, as well as the direction and Speed of the Wind. These factors must be considered when planning or predicting travel times and distances.

Figure 17: Vehicle at different conditions.

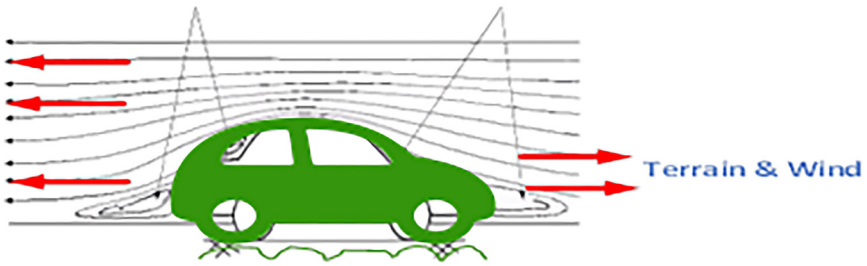

Figure 18: Terrain and wind.

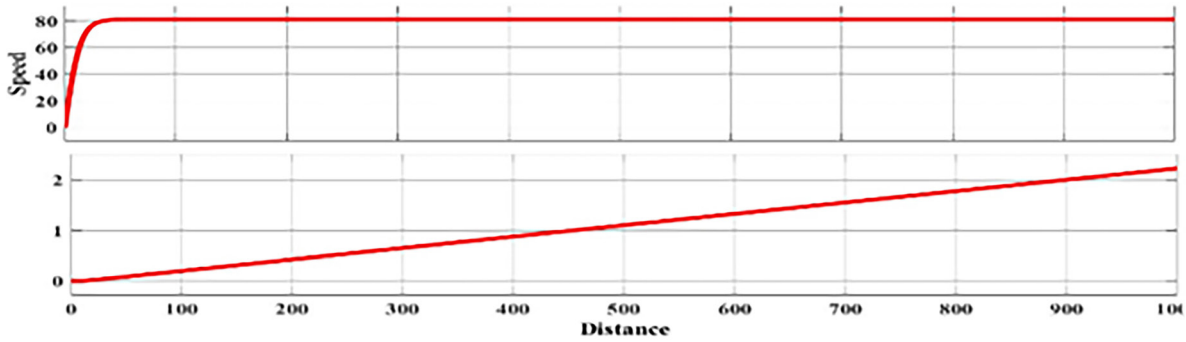

Figure 19: Speed and distance of terrain & wind.

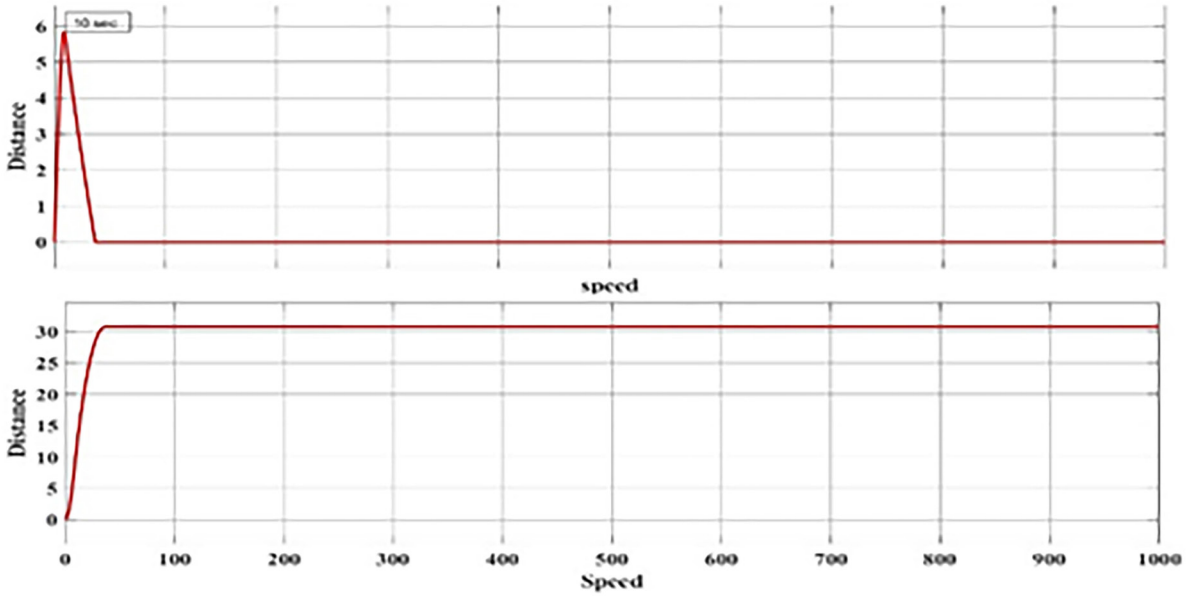

Figure 20: Vehicle characteristics.

The vehicle slope is until 10 seconds after the speed increases. The vehicle speed is then lowered to 10 seconds. The vehicle's speed is zero when it reaches a flat surface. Additionally, the distance traveled is restricted to 30 meters. There is no breaking mechanism on this. A weighted contact rotating friction block called the Break Design uses normal force to replicate friction between two spinning surface loads. The effective torque radius is 280 mm [49].

The breaking mechanisms, which are the systems or parts in charge of halting or slowing down a moving item, are shown in Figure 21. They are vital in many areas, such as production, transportation, and daily living. Eddy Current brakes: A braking force is produced when magnetic fields cause currents to flow through a moving conductor. A braking force is created when magnetic particles are suspended in a fluid and exposed to a magnetic field [50].

Figure 21: Breaking mechanism.

6.1. With breaking mechanism

Figure 22 represents the tyre force applied to the 30^0, as shown in the above waveform. When the beak is used at 30^0, the Vehicle comes to zero, the torque also falls, and Speed and reduced force will come to negative.

7. MODELLING FOR BOOST CONVERTER

A boost converter is a DC-DC converter that boosts the input voltage to generate a greater output voltage. It usually consists of an inductor, a switch, a diode, and a capacitor. The basic system includes charging the indicator when the switch is open and increasing the voltage. The mathematical equations that describe the behavior of its components, such as the inductor's voltage and current relationship, the switch's ON-Off behaviors, and the diode characteristics, can be derived from the principles of circuit Analysis, such as Kirchhoff's law and the equation (Figure 23).

Converting one type to another is known as DC-to-DC conversion, and solar panels, rectifiers, batteries, and DC generators can produce it. Step-up conversion is the Process of boosting the supply voltage in a DC-DC converter by producing an output voltage that is higher than the source voltage. Due to the necessity of converting electricity, the output current is lower than the source current. The key elements of a converter circuit are shown [51].

7.1. Quadratic boost converter

A quadratic boost converter is a DC-DC converter that can increase the voltage output ratio by four times greater output voltage. Typically, they must change the converter's duty cycle to ensure it performs within its stated voltage and current requirements. Designing a Specific Boost Converter requires careful consideration of the Output and input Current and Voltage requirements and the choice of components and Control Strategy. It is often a Complex Engineering task that may require simulation and iteration to achieve the desired Performance for different Voltages.

Figure 24 represents a quadratic boost converter, a DC-to-DC converter that can increase the input voltage to a significantly higher output voltage. It's characterized by its unique topology, which involves multiple voltage amplification stages. The topology of a quadratic boost converter typically consists of a series of stages, with each stage adding to the output voltage. The switches in each stage are controlled in a specific sequence to achieve the desired voltage amplification [52] (Tables 3 to 7).

The Boost converter is emulated using MATLAB 2024, and the circuit is presented. The circuit's input voltage is 10V, operating at a switching frequency of 1KHz. The duty ratio is altered to boost the output voltage to the desired value.

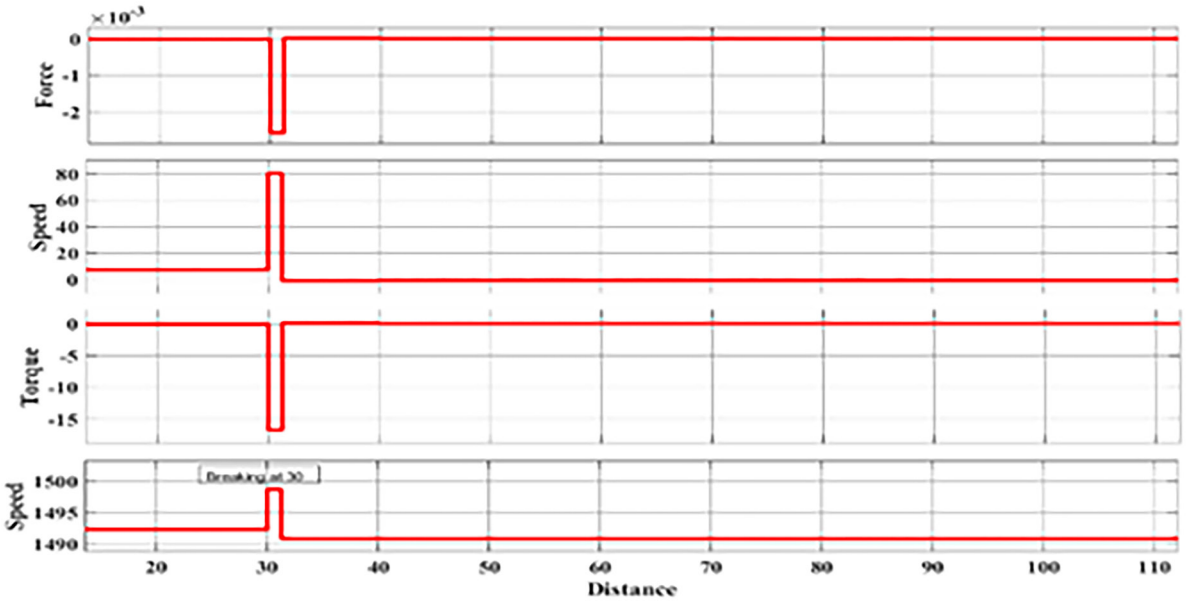

Figure 22: With the breaking mechanism.

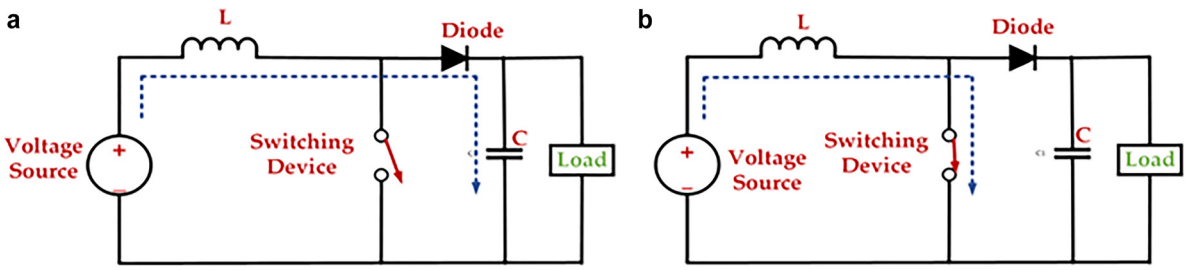

Figure 23: Circuit diagram of boost converter; (a) Switch off (b) Switch on.

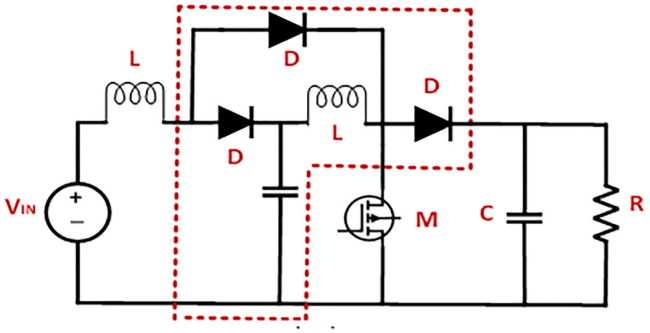

Figure 24: Quadratic boost converter.

Table 3: Specifications.

S. NO	SPECIFICATIONS	VALUES
1	Capacitor	400e-6
2	Inductor	4e-3
3	Resistance	10.44Ω
4	Voltage	30V

Table 4: Quadratic boost converter.

S. NO	INPUT		OUTPUT		POWER
	VOLTAGE	CURRENT	VOLTAGE	CURRENT	
1	10V	13A	38.9V	3.6A	138.8W
2	15V	26A	59.2V	5.671A	335.1W
3	20V	28A	80.35V	7.696A	618.4W
4	25V	35A	101.5V	9.721A	986.6W
5	30V	42.8A	122.6V	11.75A	1441.2W

Table 5: Analysis of output boost converter.

DUTY RATIO	BOOST- CONVERTER				
	INPUT VOLTAGE	INPUT CURRENT	OUTPUT VOLTAGE	OUTPUT CURRENT	EFFICIENCY
0.3	10	4	12.34	1.245	38.40%
0.6	10	8.2	20.14	2.4534	60.24%
0.8	10	15.24	33.45	3.345	73.41%

Table 6: Analysis of quadratic converter boost converter.

DUTY RATIO	QUADRATIC BOOST- CONVERTER				
	INPUT VOLTAGE	INPUT CURRENT	OUTPUT VOLTAGE	OUTPUT CURRENT	EFFICIENCY
0.3	10	0.4	14.5	0.145	52.62%
0.6	10	2.04	37.45	0.3745	68.84%
0.8	10	9.25	90.25	0.9025	88.054%

Table 7: Comparison of efficiency.

DUTY RATIO	EFFICIENCY	
	BOOST-CONVERTER	Q- BOOST CONVERTER
0.3	38.40%	52.62%
0.6	60.24%	68.84%
0.8	73.41%	88.054%

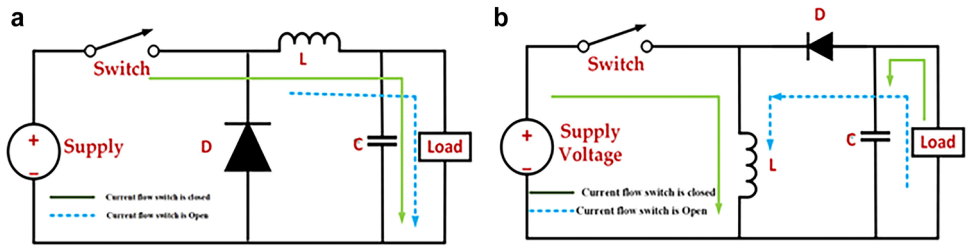

Figure 25: (a) Buck converter, (b) Buck-boost converter.

The switching pulse is given to the switch to transfer the maximum Output to the Load from the given to the switches, and then there will be some stress on the switches [53].

7.2. Buck-boost converter

A buck-boost converter may increase or decrease the input voltage to maintain a consistent output voltage. These topologies incorporate the configurations of both the buck and the boost converters. A buck-boost converter can operate two unique conduction modes, e.g., continuous and discontinuous. Figure 25 representation the modes are based on how the inductor current behaves during the switching cycle. Battery-powered and renewable energy systems are applications in which the input voltages vary widely, and the Output needs to be regulated.

The boost, buck-boost, and quadratic boost DC-DC converters control voltages in DC-DC conversion. Each has specific advantages and is chosen according to the individual's demand. The boost, buck-boost, and quadratic boost DC-DC converters regulate voltages in DC-DC conversion; each has unique advantages and is determined based on the specific requirement [54].

8. PROPOSED BLOCK DIAGRAM

A hybrid system diagram for energy storage is shown in Figure 26. A Permanent Magnet Synchronous Motor (PMSM) load is powered by this system, which combines solar photovoltaic (PV) panels, a battery, and a super-capacitor. A DC-DC boost converter links the PV panel to the load. A boost converter extracts the greatest power from the PV panel. The perturbation and observation method is used in this instance for MPPT. DESS uses bi-directional DC/DC converters to connect to the load. DESS maintains a steady output voltage (Vdc) when the generation and demand are not aligned. A deviation from the reference value occurs when the market size surpasses the generation size. The release of HESS will meet the extra demand.

Similarly, V_{dc} increases from its reference value when the market is less than the generation. Therefore, HESS will be charged to absorb the surplus Power. The buck-boost converter is a bi-directional converter that facilitates the power flow between the Load and HESS. This paper presents the Load as a PMSM Motor. Our

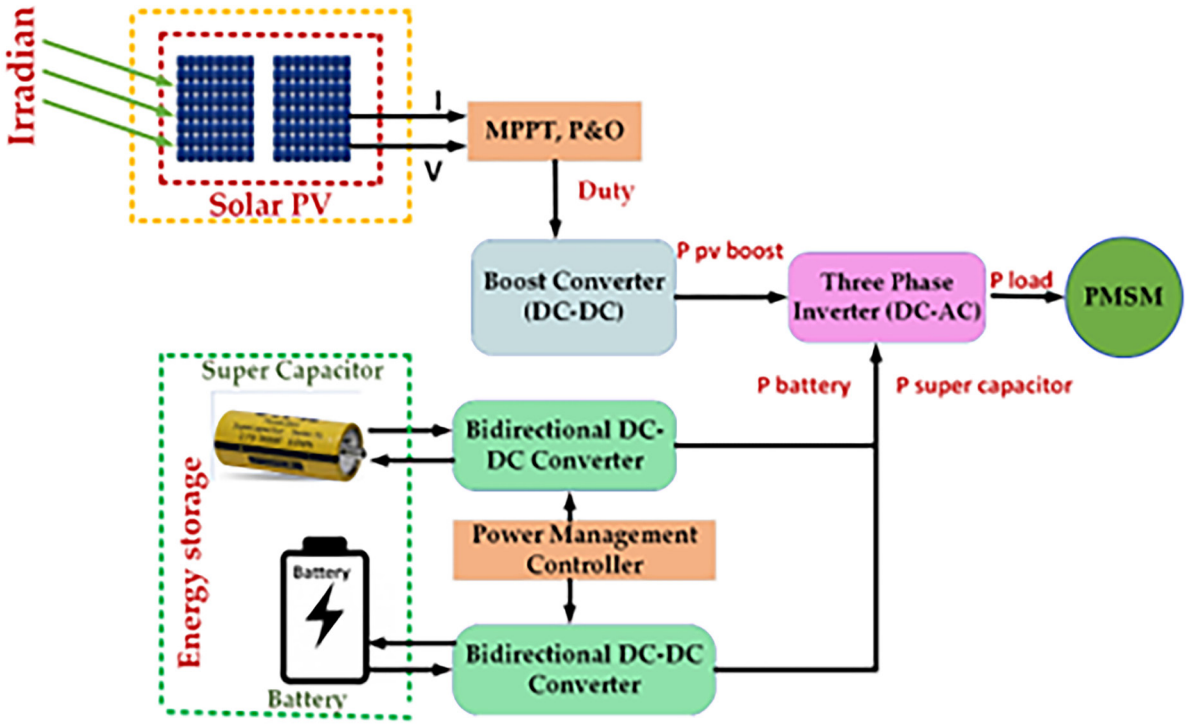

Figure 26: Proposed block diagram for the PV, Battery, and supercapacitor-based dual energy storage system (DESS).

system stores electrical energy using a battery and a supercapacitor; thus, the acronym HESS stands for Hybrid Energy Storage System.

The key elements in the block diagram above are the MPPT controller, buck-boost converter, and PV module boost converter. The intermediate boost converter can be connected to the DC power supply provided by the PV module. PV power enters the DC to A.C connection, meets the load power need, and is either used by the load motor or stored in a battery with more capacitor support. Supercapacitors, both internal and external, provide power to a load, while boost converter batteries regulate the battery's power output [55].

During sunny periods, the PV panels generate electricity, which can power the PMSM motor directly or charge the hybrid Battery and Supercapacitor. The hybrid battery stores excess energy from the PV system for later use when the sun is not shining, ensuring a continuous power supply to the motor [56].

Figure 27 represents the DC-decoupled aspect, which refers to the fact that the energy storage elements (supercapacitor and battery) are connected to the DC side of the inverter through separate DC-DC converters. This provides flexibility in managing the power flow between the PV source, energy storage, and the AC load. The transformer less characteristic implies that no high-frequency transformer is used within the inverter stage for isolation, which can improve efficiency and reduce size and cost. Still, it requires careful consideration of safety and grounding.

The Supercapacitor can provide rapid bursts of Power when the motor requires additional energy, such as during acceleration or sudden load changes. This helps optimised the motor's Performance and efficiency. An intelligent control system regulates energy flow inside the PV system [57]. Hybrid Battery and Supercapacitor to maximize efficiency, decrease energy waste, and assure a steady power supply to the PMSM motor.

8.1. MPPT controller

The MPPT control algorithm is generally used to extract the maximum capability of the PV module's Power concerning solar irradiance and temperature at a particular instant by the MPPT controller. An efficient method for tracking maximum PowerPoint has been developed. In this paper, the perturb & observe method is used for MPPT. In this, the incremental change in the value of power P is measured as the value of P is negative. The direction of voltage adjustment is reversed, and the operating point is tried to make it closer to the MPP value. The flow chart algorithm is shown below.

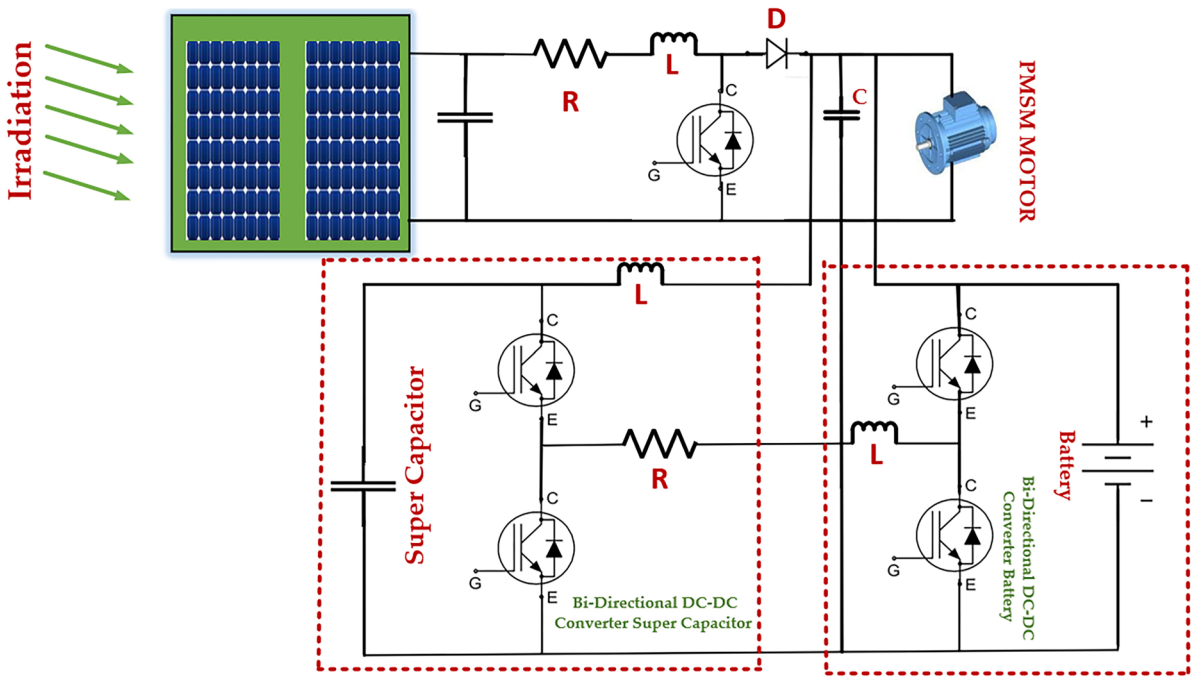

Figure 27: DC-decoupled type single-phase transformer less PV inverter system.

8.2. Solar PV panel

A photovoltaic (PV) array consisting of several modules is a fundamental power conversion unit for a PV generator system. The photovoltaic (PV) cell is a p-n junction fabricated in a thin semiconductor wafer. Solar Power is directly converted to electricity through the photovoltaic effect. Waree Energies W.U.- 120 is used for MAT/LAB purposes [58] (Table 8).

Solar cells use sunlight to generate electricity, as seen in Figure 28. The current-voltage (V-I) and power-voltage (P-V) curves, which offer important details about the cell's Output under various circumstances, such as differing irradiations, are frequently used to characterize their performance. The V-I curve moves to the right and upward as irradiation rises. This indicates that the solar cell generates more voltage and current at all voltage levels.

Table 8: Solar panel module specifications.

CHARACTERISTICS	SPECIFICATIONS
Typical extreme power (Pmpp)	120.7W
Voltage at extreme power (Vmp)	17V
Current at extreme power (Imp)	7.1A
Short-circuit (Isc)	8A
Open circuit voltage (Voc)	21V
Temperature coefficient of open circuit voltage	0.358 (%/0.C)
Temperature coefficient of short circuit current	0.052 (%/0.C)
Approximate effect of temperature on power	−(0.5 ± 0.015) (%/0.C)
Fuse rating	25A
Tolerance of power	0 ± 3%
Type	Mono-Crystalline
Module efficiency STC (%)	21.48%
Maximum voltage	1000/1500 VDC

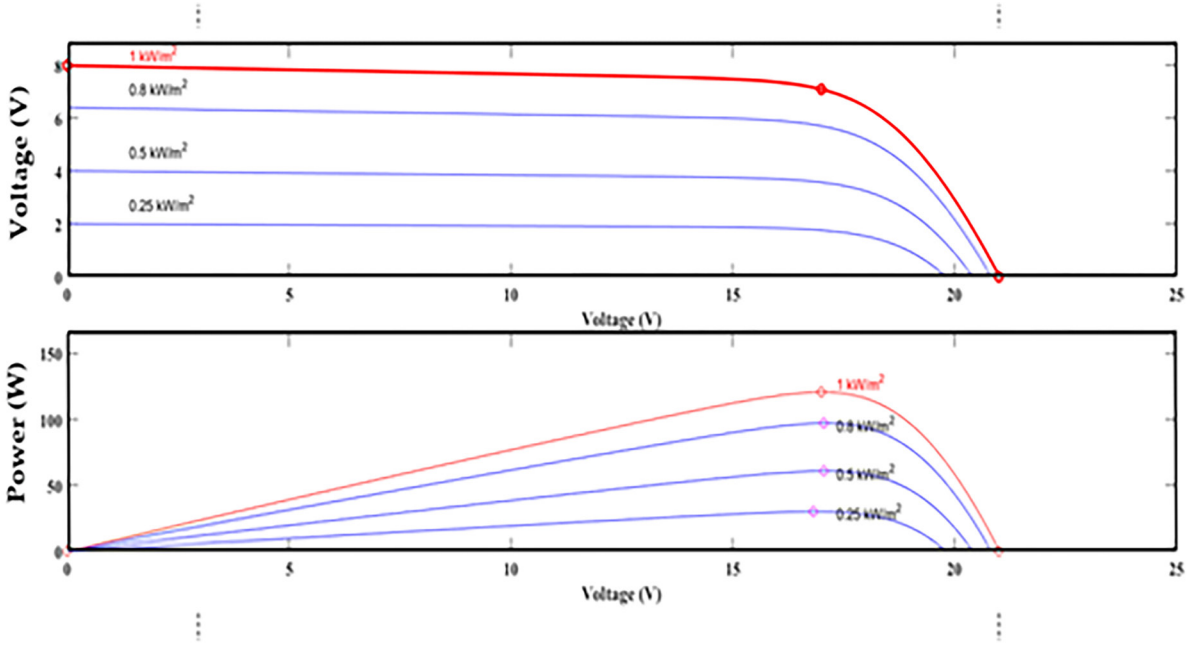

Figure 28: V-I And P-V family curves for different irradiations [59].

8.3. Control of Permanent Magnet Synchronous Motor (PMSM) drive

The control approach employed in this study to manage the PMSM speed is the dq control method, which uses Clark's and Park's transformation to control and transform parameters. The PMSM receives the inverter's step input torque and three-phase output voltage [60]. The Output of PMSM includes stator line currents (Ia, Ib, Ic), rotor speed (ωe), electromagnetic torque (Te), and rotor angle (Θ). The rotor speed is compared with the reference speed, and the error is fed to a PI controller, generating the Iq_Ref current. By applying the inverse Park's transformation, Iabc_Ref is generated. Iabc_Ref and Iabc (feedback taken from PMSM stator output terminals) are compared in the PWM Inverter, and the PWM inverter generates three-phase voltages Va, Vb, and Vc, and these three-phase voltages are given to PMSM input terminals from which the rotor speed is regulated as shown in Figure 29.

8.4. Control scheme for battery and supercapacitor

Batteries provide high energy density but slower Charging and discharging rates. Supercapacitors offer high power density but lower energy density compared to batteries. Combining batteries and supercapacitors can leverage their strengths, improving overall Performance [61].

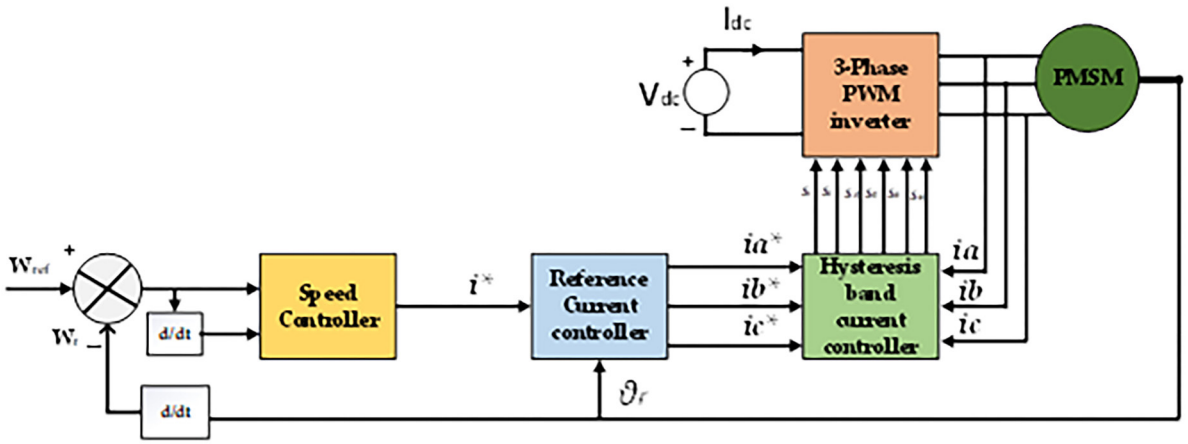

Figure 29: Block diagram of PMSM Drive.

Table 9: Control scheme for battery and supercapacitor equations [63].

	BATTERY	SUPER CAPACITOR
State of Charge (SOC)	$SOC_b = \frac{Qb(t)}{Qb,\ max}$	$SOC_c = \frac{Qc(t)}{Qc,\ max}$
Voltage	$Vb = f(SOC_b)$	$Vc = \frac{Qc(t)}{C}$

Table 10: Control scheme and equation.

S. NO	CONTROL SCHEME AND EQUATION	
1	Voltage equation	Passive Balancing: $Rb = \frac{Vb - Vc}{Ib}$ Active balancing: $Pbal = (Vb - Vc) \cdot Ibal$
2	State of Charge (SOC)	Coulomb Counting: $SOC(t = SOC(0) + \frac{1}{Qmax} \int 0ti(\tau)d\tau$ Open-Circuit Voltage (OCV): SOC = f(OCV) Model-Basedstimation: SOC = g(V, i, T)
3	Power Sharing	Constant Power Sharing: Pb = Pref and Pc = Ptotal − Pb Constant Current Sharing: ib = iref and ic = itotal − ib Voltage-Based Sharing: $Pb = \frac{Vb}{Vb + Vc}$. Ptotal and $Pc = \frac{Vc}{Vb + Vc} \cdot Ptotal$ Power-Based Sharing: $Pb = f(SOC_b, SOC_c, Ptotal)$
4	Control Strategies	Charge-Sustaining Strategy: $SOC_b = SOCref$ Power-Sharing Strategy: $Pb = f(SOC_b, SOC_c, Ptotal)$ Peak-Shaving strategy: Pc = f(Pgrid, Pload)

Note: Q: Charge (Ah) V: Voltage (V) i: Current (A) R: Resistance (Ω) P: Power (W) C: Capacitance (F) T: Temperature (K), SOC ref: Reference SOC, Pref: Reference power, i_{ref}: Reference current, P_{grid}: Grid power, P_{load}: Load power.

- Voltage Balancing: Ensures uniform voltage distribution across the cells to prevent overcharging or undercharging. Passive balancing (resistors or diodes), Active balancing (using power electronic circuits).
- State of Charge (SOC) Management: Determines the charge level of each component. Coulomb counting, Open-circuit voltage (OCV), and Model-based estimation.
- Power Sharing: Allocates Power between the Battery and the Supercapacitor based on specific criteria. Constant power-sharing, Constant current sharing, Voltage-based sharing, power-based sharing.
- Predictive Control: Uses system models and future predictions to optimise control decisions. Model Predictive Control (MPC) and Adaptive Predictive Control (APC). During acceleration, the Supercapacitor provides rapid Power for quick acceleration. During cruising, the Battery supplies steady Power. During regenerative braking, both components can be used for energy recovery.

The optimal control scheme depends on the specific application and the desired performance objectives. By carefully considering the abovementioned factors, engineers can select a control strategy that effectively manages the Battery and Supercapacitor in a hybrid energy storage system [62] (Tables 9 and 10).

9. SIMULATION RESULTS

This system model sends solar PV array power to a boost converter, which improves the DC voltage generated and filters out undesired transients during PV generation. The boost converter output is sent to the storage unit, which includes a DC-DC converter, a battery supercapacitor, and a hybrid storage unit. When the vehicle is connected, the energy in the storage unit is used to recharge [64].

The MATLAB/Simulink-validated control technique for variable solar irradiation and constant temperatures is shown in Figure 30. The Simulink model produced various simulation results, which are displayed

below in three groups. One for the Output of the PV, battery, and supercapacitors [65]. The objective is to maintain the output voltage at V_{Ref} = 50 V even if the irradiance is reduced. The battery's initial State of Charge (SOC) is set at 50%. Output results.

Figure 31 represents that the PV voltage remains almost constant over the given time range is 42.6V. The PV module is operating near a fixed voltage point, possibly controlled by a Maximum Power Point Tracking algorithm or a constant voltage control strategy. Initially, the PV current is steady at around 100A. The plots depict a PV system where voltage is held constant, current suddenly increases at a specific moment, and power output rises accordingly. MPPT operation shifting to a higher power point.

Figure 32 represents the voltage stays nearly constant around 55V the plots indicate that the supercapacitor is mostly in a steady, high-voltage, high-SoC state, with a small event around 0.032 s causing a temporary current drop and a slight voltage rise.

Figure 33 represents the PV system quickly reaches 1000 W and stays stable, with minor oscillations. The supercapacitor handles the transient high-power demand, protecting the battery from sudden load changes. Over time, the battery provides steady power while the PV system maintains constant generation to meet the load and recharge the storage.

10. EXPERIMENTAL OPAL-RT RESULTS

The above Figure 34 shows the rotor speed (in m/s) versus time, with a note indicating it is set constant at 700 rpm.The rotor starts from near zero speed. After reaching the target speed, it stays almost constant, indicating

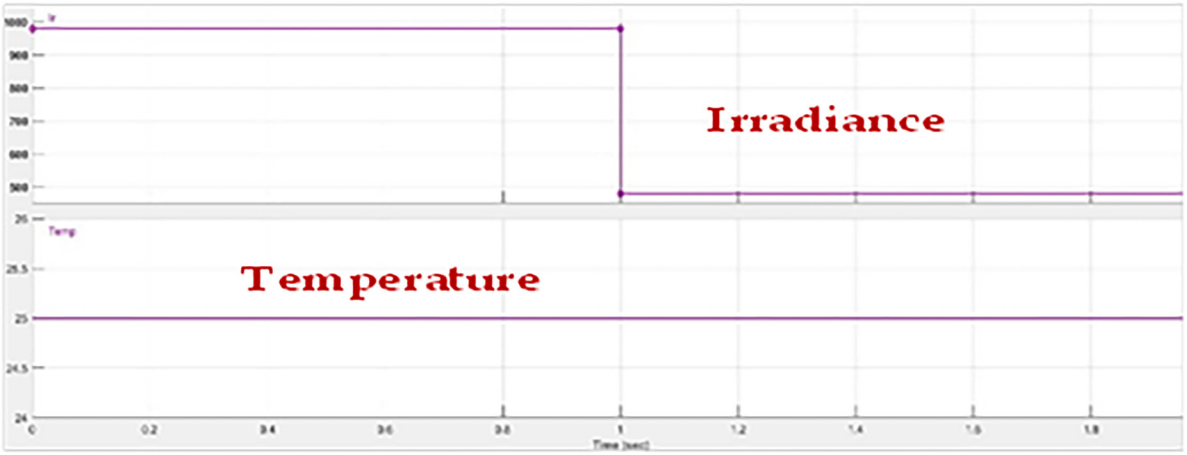

Figure 30: Temperature and irradiance input to PV Array.

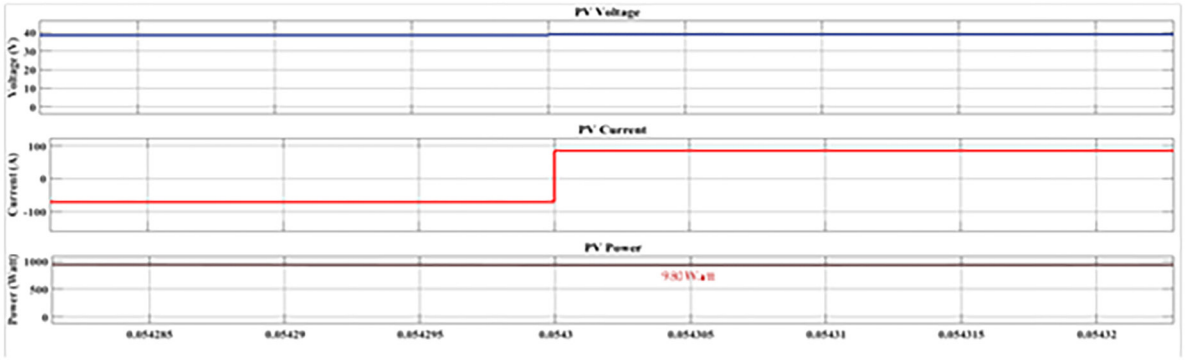

Figure 31: PV Voltage, PV Current, and PV Power.

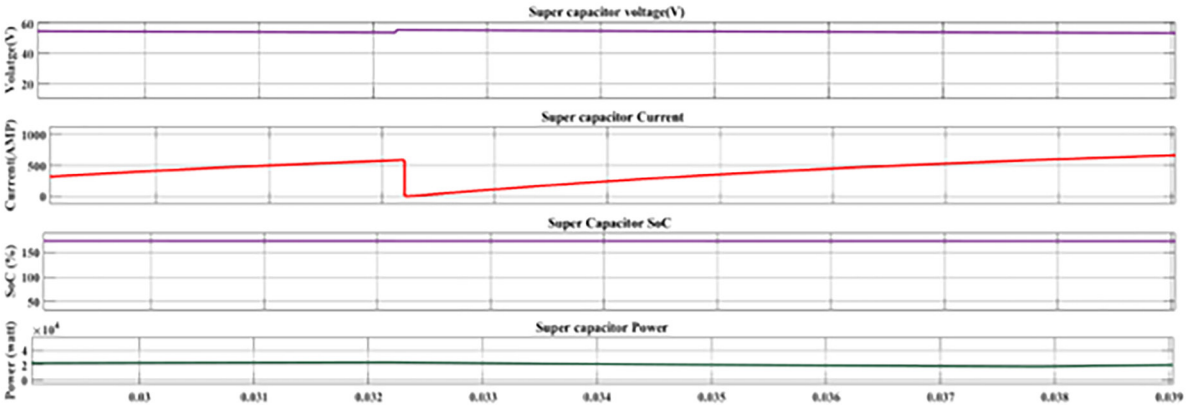

Figure 32: Voltage, current, %Soc, and power of supercapacitor.

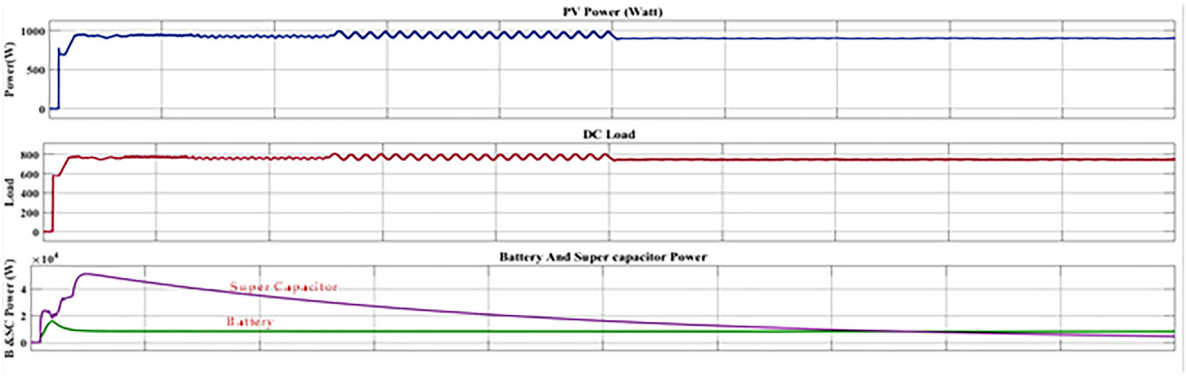

Figure 33: Waveforms of PV power, DC load power, battery power and supercapacitor power.

stable operation at 700 RPM, with only minor fluctuations. The system successfully accelerates the rotor to the set speed and maintains it, confirming proper speed regulation.

The Figure 35 shows the rotor speed (m/s) over time with a setpoint of 900 rpm. Rotor begins at near zero speed. Once target speed is reached, it remains stable at 900 RPM with negligible fluctuations, indicating effective speed control. The system smoothly accelerates and maintains the rotor at the desired 900 RPM operating point.

Figure 36 represents the torque plot represents a load disturbance test, where a step load is applied and then removed to see how the system handles sudden changes in mechanical demand. The short duration of the high torque period suggests a transient load change, used for testing the system's dynamic response.

Figure 37 illustrates the behavior of a solar PV system under varying irradiation conditions. PV current increases proportionally with irradiation since higher sunlight produces more current from the PV array. PV

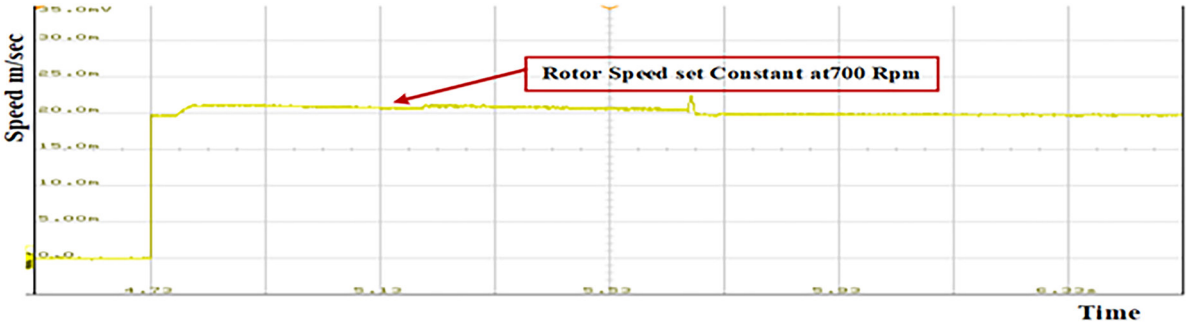

Figure 34: Reference rotor speed set constant at 700 Rpm.

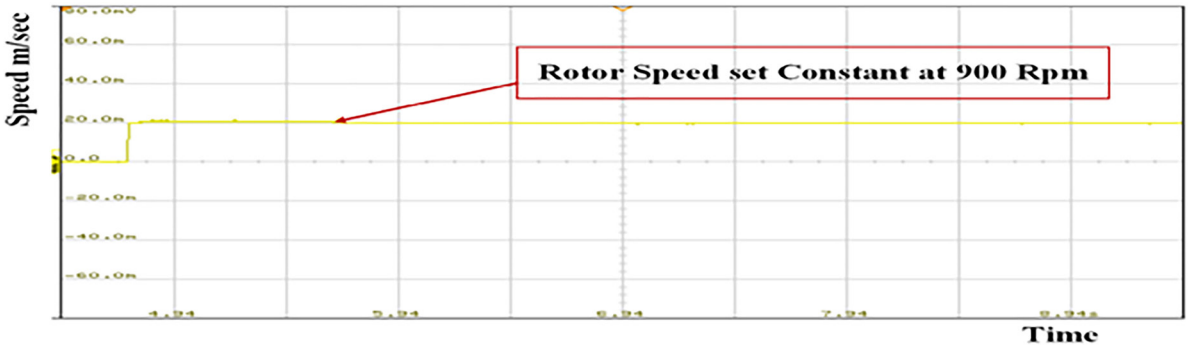

Figure 35: Rotor output speed remains constant at 900 Rpm.

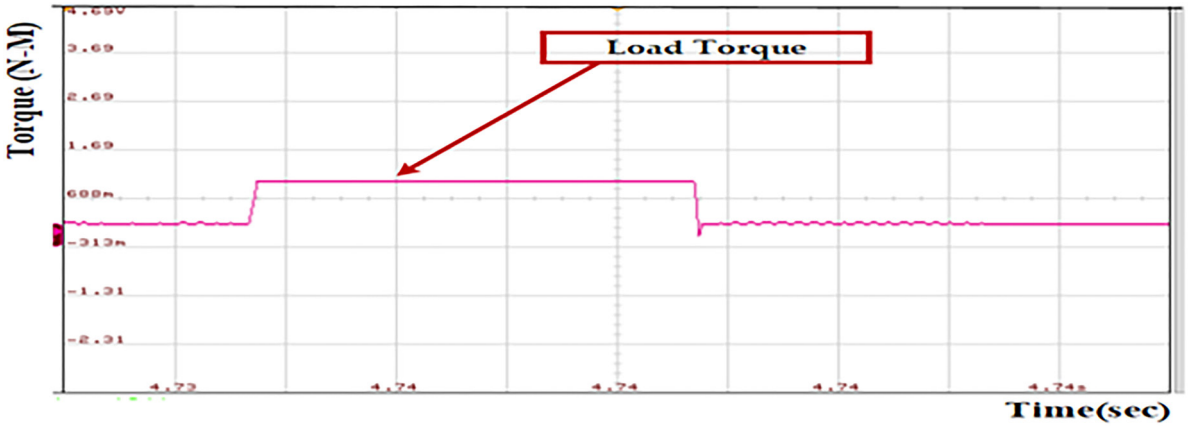

Figure 36: Wave forms of the stator of the PMSM load torque.

output power is directly dependent on solar irradiation while the load remains constant. As irradiation increases, PV current and power rise, maintaining supply to the DC load and potentially charging storage devices when excess power is available.

Figure 38 shows the electrical characteristics and state of charge (SoC) of a supercapacitor during operation. Voltage remains relatively constant, with small variations during current changes, indicating stable opera-

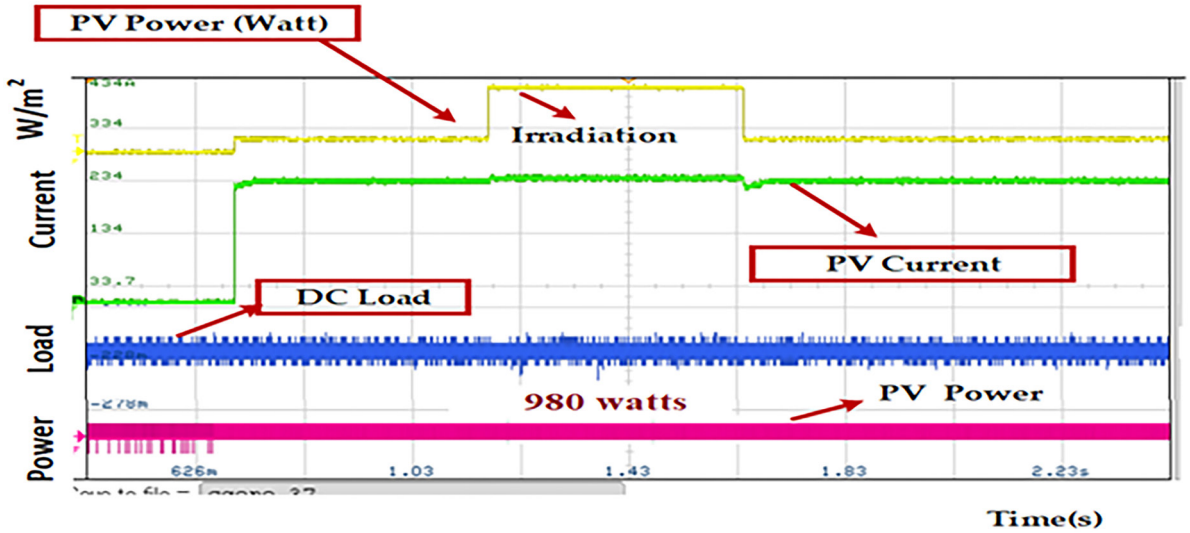

Figure 37: Wave forms of the solar pv voltage, current and power.

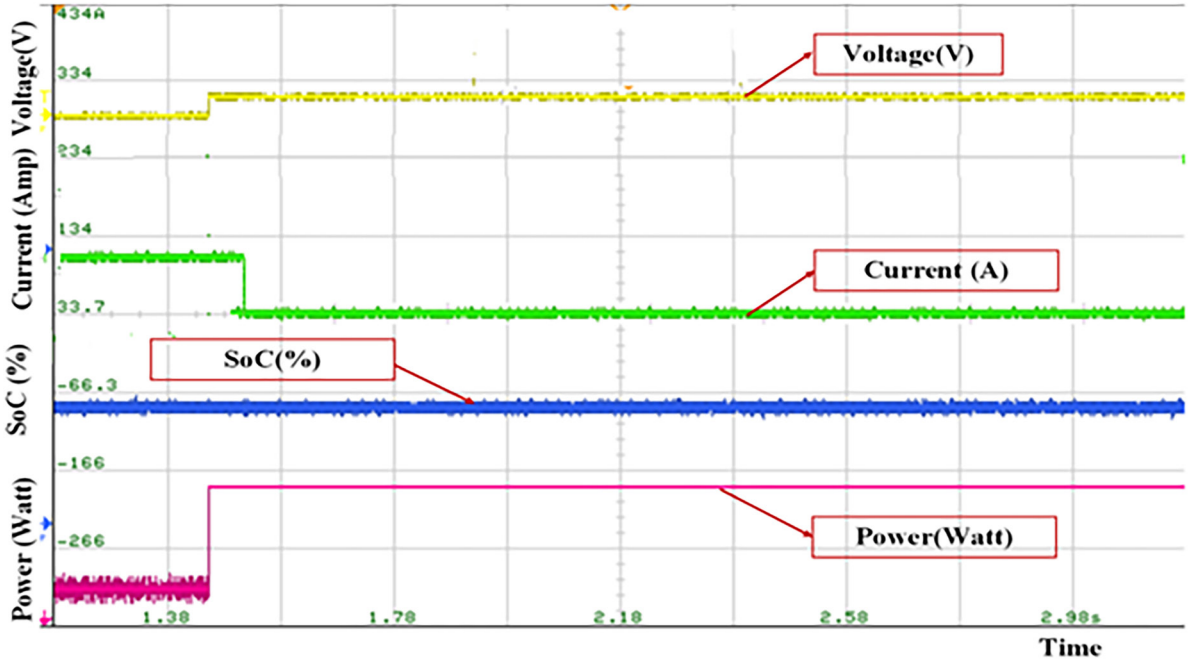

Figure 38: Wave form of voltage, current, %soc, and power of supercapacitor.

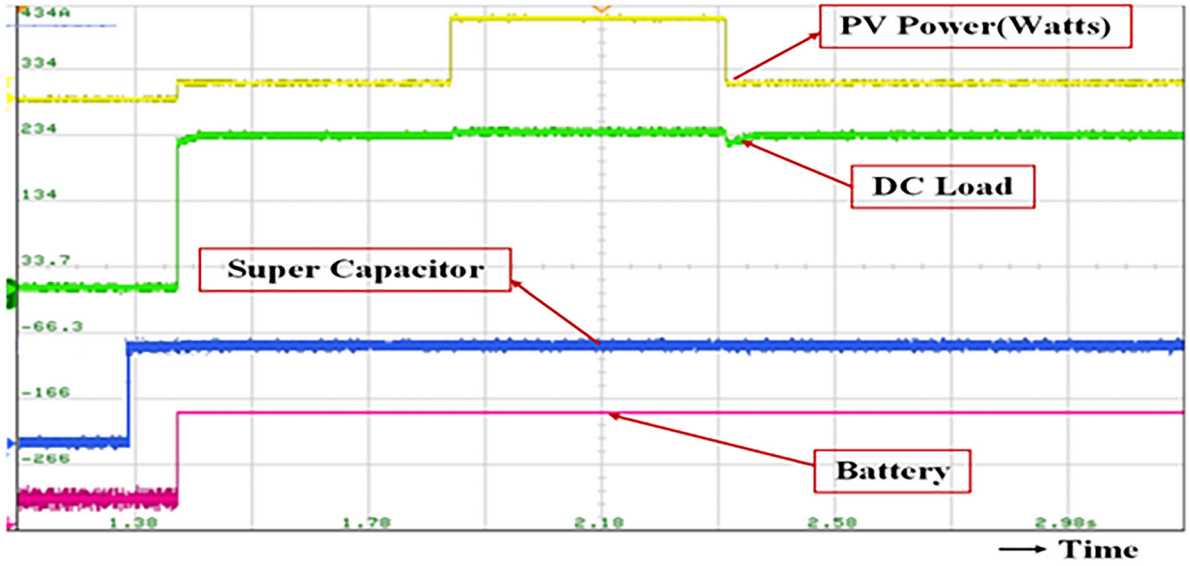

Figure 39: Waveforms of PV power, DC load power, battery power and supercapacitor power.

tion under charge/discharge cycles. An initial lower current increases to a higher value, then stabilizes, reflecting load changes or charging control actions. SoC remains almost steady throughout the period, showing that the supercapacitor is operating within a high charge range and no deep discharge is occurring. Power Remains steady afterward, reflecting constant load supply. The supercapacitor responds instantly to current changes, delivering stable voltage and maintaining a high SoC. This confirms its role in providing quick power bursts and supporting the system during load variations without significant energy depletion.

Figure 39 illustrates how power is shared between the PV source, battery, and supercapacitor to supply the DC load under changing irradiation. Increases in steps with higher solar irradiation and decreases when sunlight reduces. Remains constant, indicating steady load demand. Supplies steady backup power, compensating for PV variations once the supercapacitor stabilizes. The PV system is the primary source, while the supercapacitor handles transients and the battery ensures long-term power stability.

11. EXPERIMENTAL SETUP

Figure 40 represents the Hil Simulator in a real-time system. Input source 1 PV Simulator is a device that likely emulates the electrical characteristics of a photovoltaic (PV) panel, acting as the power source for the system. A battery is an energy storage device that can be used to supply or absorb power in the system. The Super Capacitor is an energy storage device known for its high-power density and fast charging/discharging capabilities. Proposed converter: This is the central component being tested. It's a power electronic converter designed to transform electrical energy from one form to another. A voltage probe is a measurement device used to measure the voltage at different points in the circuit. A current investigation is a measurement device used to calculate the current flowing through various parts of the circuit. dSPACE RT 1104: This is a real-time control system used for controlling the converter and acquiring data. It's a powerful tool for rapid prototyping and hardware-in-the-loop simulations. An electronic instrument used to visualize and analyses the waveforms of voltage and current signals in the circuit. PC is used to control the DSPACE system, acquire data, and display results. A load is an electrical component or system that consumes the power output from the proposed converter. This setup suggests an experiment involving a power converter with potential applications in renewable energy systems (due to the PV simulator) and energy storage (battery and supercapacitor). The dSPACE system and DSO are crucial for analysing the performance and behaviour of the proposed converter under different operating conditions.

Steps:

- The power management is developed based on the availability of input sources and the power demand of PMSM. In Simulink/D-SPACE, initially set the carrier frequency to 10000 Hz, the duty cycle to 0.5, and the clock frequency to 40 MHz. Based on the duty cycle of the boost converter, the DC bus voltage is maintained at 48 V, and the controller enables the relay switches. (available power from sources).
- PMSM gets power through the inverter and starts to rotate. Keeping the 48 V in the DC bus is measured through the Digital Signal Oscilloscope (DSO) device and the DC bus voltage measured through the DSO. The monitor is required and load power of PMSM, and it controls the ON/OFF function of relay switches as per the availability priority.
- The adjustment of the rheostat provides the load variation in the PMSM through the DC motor. The controller senses the load power and matches the load power with the input source power. Based on the power changes in the PMSM (load) sources, input sources give the power to the load using relay switches as per the command from Simulink/D-SPACE.
- The proposed work compares the design types of motors and MPPT controllers, vehicle dynamics of terrain method, control methods, and implementation of various drive cycles (Table 11). An MPPT controller and the vehicle dynamics design for error-free, simple power calculation help the power management with an instantaneous reference current technique to find the maximum energy sources [67].

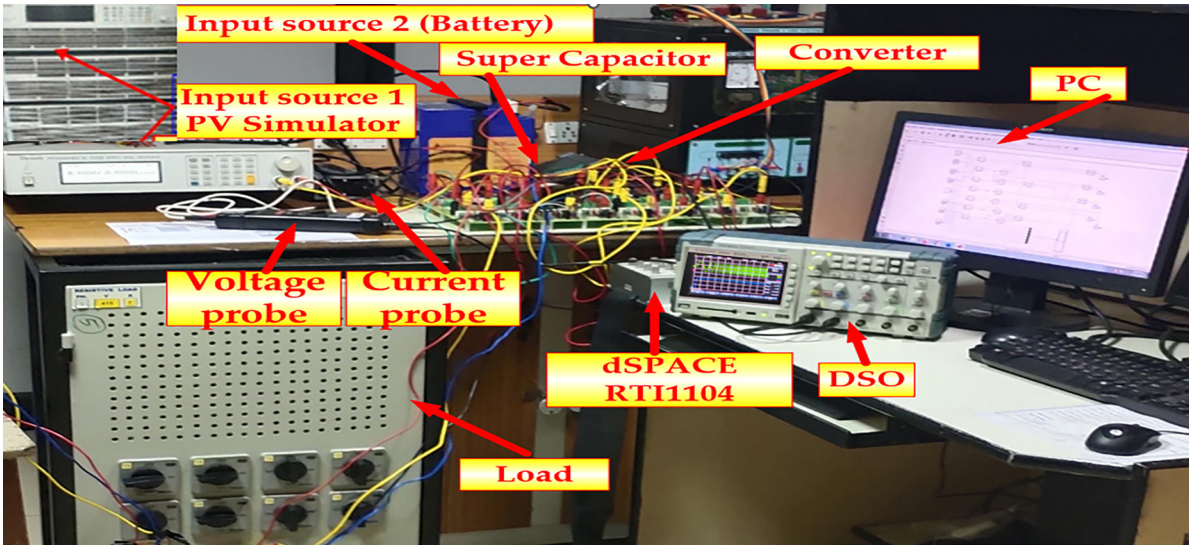

Figure 40: Photograph of the HIL simulator in a real-time system.

Table 11: The proposed work compares the sources used in the control methods and implementation of varying drive cycles [66].

REF	SOURCE 1	SOURCE 2	SOURCE 3	CONTROL METHOD	MPPT	DETAILED VEHICLE DYNAMICS	MOTOR TYPE	NO OF MOTORS	COMPARED WITH OTHER ARTICLE	SELF-CHARGING
SHARF *et al.* [44]	Fuel Cell	Super Capacitor	–	Robust Optimisation.	No	No	PMSM	2	✗	✗
LANG *et al.* [45]	Fuel Cell	Battery	–	Online robust EMS	No	Yes	-	1	✗	✗
AZADMANJIRI *et al*. [46]	Fuel Cell	Battery	–	Perturbation Simulation	No	No	IM	-	✓	✗
XIAO *et al*. [47]	Battery	–	–	DTC	No	No	-	2	✗	✗
TIFIDAT and MAOUHOUB [48]	Battery	Hydraulic pump Motor	–	Optimization Proximal	No	Yes	-	1	✗	✗
THOUNTHONG *et al*. [49]	Battery	Engine	Super Capacitor	Reinforcement Learning	No	Yes	-	2	✗	✗
XUN *et al*. [50]	Battery	Engine	–	Dynamic Programming	No	Yes	-	2	✗	✗
KALAIVANI and JOICE [51]	Solar	Battery	Fuel cell	Digital	Yes	No	PMSM	1	✓	✓
Proposed	Solar	Battery	Super Capacitor	Simulation Perturbation	Yes	Yes	PMSM	1	✓	✓

Table 12: Comparison of performance parameters.

PARAMETER/PERFORMANCE	SINGLE BATTERY SYSTEM (LI-ION)	INTEGRATED SYSTEM (LI-ION + SUPERCAPACITORS)
Energy density	High	Moderate
Power density	Moderate	High
Charging time	Longer	Shorter (due to supercapacitors)
Cycle life	Limited	Extended (due to reduced strain on batteries)
Peak power handling	Moderate	High
Regenerative braking efficiency	Moderate	High
Operational cost	Higher	Lower (due to longer battery life and efficiency)
Thermal management	Complex	Simplified (due to lower battery strain)
Maintenance requirements	Higher	Lower (due to extended battery life)

Table 13: Comparison of performance parameters for cost analysis of integrated system vs. Single battery system.

SYSTEM TYPE	BATTERY COST	SUPERCAPACITOR COST	SOLAR PANEL COST	ENERGY SAVINGS	BATTERY LIFESPAN INCREASE	ESTIMATED COST REDUCTION (%)
Battery Only	High (₹10,18,000 per MWh)	_	_	Baseline	Baseline	0%
Integrated System	Medium (Fewer replacements) ₹10,18,000 per MWh	Additional cost	Additional cost (₹25,000 - ₹50,000 per kW)	15-30% (Solar + Regen)	30-50% increase	20-40% over lifetime

Table 12 clearly compares the single battery system and the integrated system, highlighting the various advantages in terms of energy density, power density, charging time, cycle life, peak power handling, regenerative braking efficiency, operational cost, thermal management, maintenance requirements, cost of energy, and annual savings.

Table 13 represents the cost analysis of a single battery and an integrated system. The cost of battery-based energy storage in India is approximately ₹10.18 per kWh. Solar Panel Costs In India, as of 2025, photovoltaic panel prices range from ₹25 to ₹50 per. Therefore, a 1 kW solar system would cost between ₹25,000 and ₹50,000. Despite its higher initial cost, the integrated system offers significant savings (20–40%) in the long run by reducing energy consumption and battery replacements. This makes it a more sustainable and cost-effective solution compared to a single-battery system. Integrating solar panels and supercapacitors with battery systems presents a higher initial investment. However, the substantial benefits in energy savings and extended battery lifespan contribute to significant cost reductions over time, making the integrated system a more economical and sustainable choice in the long run.

12. CONCLUSION

The proposed hybrid or dual-energy storage system (DESS) is designed to ensure the continuity of power supply to the PMSM motor. Using a capacitor decreases stress on the Battery and increases its lifespan. Solar PV panels provide vehicles with a sustainable energy source, lessening their dependence on non-renewable sources and reducing carbon emissions. These technologies may enhance electric automobile performance and environmental impact, paving the way for a more sustainable future. In this energy storage system, when the demand exceeds the PV-generated Power, the auxiliary sources, the Battery and Supercapacitor, get charged. The output DC voltage remains constant at 50 volts for 0.2 sec. Contrastingly, when the demand exceeds the PV-generated Power, the auxiliary sources provide the remaining Power to keep the load power constant and the DC-link voltage constant at 50 volts. This allows the automobile to accelerate with the proper torque whenever necessary. The vehicle dynamics of Wind and Terrain, with braking and without braking, are connected to the

Vehicle's wheels, which will rotate the rotor wheel irrespective of the Speed and sudden jerks in the system, making it a more accurate vehicle system than the existing one. MATLAB/SIMULINK and D-SPACE hardware 1KW PMSM to validate the system's current profile, voltage regulation, power split operation in different load conditions, and overall energy efficiency, demonstrating a significant improvement in the reliability, performance, and efficiency of electric vehicles. The proposed system achieves a DC-link voltage regulation of 48 V, improves energy efficiency by 12%, and extends battery lifetime by reducing stress currents by 18% used to better understand the DESS system's operation, which is sinusoidal with low total harmonic distortion compared to unfiltered regular hybrid energy storage systems, benefiting the PMSM motor and resulting in better overall performance of the proposed hybrid energy storage system compared to the standard dual energy storage system. The hybrid system utilises supercapacitors' fast charge and discharge properties to alleviate stress on Li-ion batteries during peak power demands. This approach prolongs the battery's lifespan while improving the overall efficiency of the energy storage system. Studies have shown that incorporating supercapacitors can significantly reduce energy consumption and maintenance costs.

Future research directions will further optimised the DESS by exploring advanced battery and supercapacitor technologies, developing more efficient power electronic converters, and implementing sophisticated control algorithms i.e., Mayfly Algorithm- technique, genetic algorithm (GA), CUKO Search, Gray Wolf, Constrained Particle Swarm Optimization (CPSO), Harmony search (HS), Flower Pollination Algorithm (FPA), pufferfish optimization algorithm, Hippopotamus optimization algorithm, arctic puffin optimization (APO), Tiki Taka Algorithm etc. Additionally, integrating the DESS with other renewable energy sources and exploring vehicle-to-grid (V2G) capabilities will further enhance the system's sustainability and economic viability.

13. ACKNOWLEDGMENTS

The authors gratefully acknowledge the support provided by the management of VIT University.

14. BIBLIOGRAPHY

[1] THANGAVEL, S., MOHANRAJ, D., GIRIJAPRASANNA, T., *et al*., "A comprehensive review on electric vehicle: battery management system, charging station, traction motors", *IEEE Access: Practical Innovations, Open Solutions*, v. 11, pp. 20994–21019, 2023. doi: http://doi.org/10.1109/ACCESS.2023.3250221.

[2] NARAYANAN, S., RAJESH, M., "A three-way DC/DC converter with tri-battery energy storage for hybrid electric vehicle system", In: *Proceedings of the 2020 International Conference on Power Electronics and Renewable Energy Applications (PEREA)*, Kannur, India, 2020. doi: http://doi.org/10.1109/PEREA51218.2020.9339817.

[3] SHIN, J., KIM, W., YOO, K., *et al*., "Vehicular level battery modelling and its application to battery electric vehicle simulation", *Journal of Power Sources*, v. 556, pp. 232531, 2023. doi: http://doi.org/10.1016/j.jpowsour.2022.232531.

[4] KOUBAA, R., BACHA, S., SMAOUI, M., *et al*., "Krichen L. Robust optimization based energy management of a fuel cell/ultra-capacitor hybrid electric vehicle under uncertainty", *Energy*, v. 200, pp. 117530, 2020. doi: http://doi.org/10.1016/j.energy.2020.117530.

[5] DHANANJAYA, M., POTNURU, D., MANOHARAN, P., *et al*., "Design and implementation of single-input-multi-output dc-dc converter topology for auxiliary power modules of electric vehicle", *IEEE Access: Practical Innovations, Open Solutions*, v. 10, pp. 76975–76989, 2022. doi: http://doi.org/10.1109/ACCESS.2022.3192738.

[6] HARINI, S., CHELLAMMAL, N., CHOKKALINGAM, B., *et al*., "A novel high gain dual input single output Z-quasi resonant (ZQR) DC/DC converter for off-board EV charging", *IEEE Access: Practical Innovations, Open Solutions*, v. 10, pp. 83350–83367, 2022. doi: http://doi.org/10.1109/ACCESS.2022.3195936.

[7] ASHOK, B., MICHAEL, P.A., "Integration of cascaded controllers for super-lift Luo converter with buck converter in solar photovoltaic and electric vehicle", *Analog Integrated Circuits and Signal Processing*, v. 118, n. 3, pp. 449–466, 2024. doi: http://doi.org/10.1007/s10470-024-02259-y.

[8] REN, Y., RIND, S.J., JIANG, L., "A coordinated control strategy for battery/supercapacitor hybrid energy storage system to eliminate unbalanced voltage in a standalone AC microgrid", *Journal of Intelligent Manufacturing and Special Equipment*, v. 1, n. 1, pp. 3–23, 2020. doi: http://doi.org/10.1108/JIMSE-08-2020-0007.

[9] SARAVANAN, S., THANGAVEL, S., "Instantaneous reference current scheme based power management system for a solar/wind/fuel cell fed hybrid power supply", *International Journal of Electrical Power & Energy Systems*, v. 55, pp. 155–170, 2014. doi: http://doi.org/10.1016/j.ijepes.2013.08.021.

[10] BARAKAT, S., OSMAN, A.I., TAG-ELDIN, E., et al., "Achieving green mobility: multi-objective optimization for sustainable electric vehicle charging", *Energy Strateg Rev.*, v. 53, pp. 101351, 2024. doi: http://doi.org/10.1016/j.esr.2024.101351.

[11] ALSHAMMARI, N.F., SAMY, M.M., BARAKAT, S., "Comprehensive analysis of multi-objective optimization algorithms for sustainable hybrid electric vehicle charging systems", *Mathematics*, v. 11, n. 7, pp. 1741, 2023. doi: http://doi.org/10.3390/math11071741.

[12] SAMY, M.M., EMAM, A., TAG-ELDIN, E., *et al*., "Exploring energy storage methods for grid-connected clean power plants in case of repetitive outages", *Journal of Energy Storage*, v. 54, pp. 105307, 2022. doi: http://doi.org/10.1016/j.est.2022.105307.

[13] GÜVEN, A.F., YÖRÜKEREN, N., SAMY, M.M., "Design optimization of a stand-alone green energy system of university campus based on Jaya-Harmony Search and Ant Colony Optimization algorithms approaches", *Energy*, v. 253, pp. 124089, 2022. doi: http://doi.org/10.1016/j.energy.2022.124089.

[14] SAMY, M.M., BARAKAT, S., RAMADAN, H.S., "A flower pollination optimization algorithm for an off-grid PV-Fuel cell hybrid renewable system", *International Journal of Hydrogen Energy*, v. 44, n. 4, pp. 2141–2152, 2019. doi: http://doi.org/10.1016/j.ijhydene.2018.05.127.

[15] ZEREG, H., BOUZGOU, H., "Forecast-integrated techno-economic optimization of off-grid hybrid renewable system in hyper-arid regions: application to Tamanrasset, Algeria", *Energy*, v. 334, pp. 137468, 2025. doi: http://doi.org/10.1016/j.energy.2025.137468.

[16] ABDELDJALIL, D., NEGROU, B., YOUSSEF, T., *et al*., "Incorporating the best sizing and a new energy management approach into the fuel cell hybrid electric vehicle design", *Energy & Environment*, v. 36, n. 2, pp. 616–637, 2025. doi: http://doi.org/10.1177/0958305X231177743.

[17] SAMY, M.M., ALMAMLOOK, R.E., ELKHOULY, H.I., *et al*., "Decision-making and optimal design of green energy system based on statistical methods and artificial neural network approaches", *Sustainable Cities and Society*, v. 84, pp. 104015, 2022. doi: http://doi.org/10.1016/j.scs.2022.104015.

[18] DJOUAHI, A., NEGROU, B., TOUGGUI, Y., *et al*., "Optimal sizing and thermal control in a fuel cell hybrid electric vehicle via FC-HEV application", *Journal of the Brazilian Society of Mechanical Sciences and Engineering*, v. 45, n. 10, pp. 533, 2023. doi: http://doi.org/10.1007/s40430-023-04437-x.

[19] DJOUAHI, A., NEGROU, B., ROUABAH, B., *et al*., "Optimal sizing of battery and super-capacitor based on the MOPSO technique via a new FC-HEV application", *Energies*, v. 16, n. 9, pp. 3902, 2023. doi: http://doi.org/10.3390/en16093902.

[20] ETEIBA, M.B., BARAKAT, S., SAMY, M.M., *et al*., "Optimization of an off-grid PV/Biomass hybrid system with different battery technologies", *Sustainable Cities and Society*, v. 40, pp. 713–727, 2018. doi: http://doi.org/10.1016/j.scs.2018.01.012.

[21] WASEEM, M., AHMAD, M., PARVEEN, A., *et al*., "Battery technologies and functionality of battery management system for EVs: Current status, key challenges, and future prospectives", *Journal of Power Sources*, v. 580, pp. 233349, 2023. doi: http://doi.org/10.1016/j.jpowsour.2023.233349.

[22] BIJU, N., FANG, H., BATT, X., "An equivalent circuit model for lithium-ion batteries over broad current ranges", *Applied Energy*, v. 339, pp. 1, 2023. doi: http://doi.org/10.1016/j.apenergy.2023.120905.

[23] VERBRUGGE, M.W., YING, R.Y., "Energy vs power relationship for lithium ion cells over a broad range of temperatures and power densities", *Journal of the Electrochemical Society*, v. 154, n. 10, pp. A949, 2007. doi: http://doi.org/10.1149/1.2767410.

[24] FAGHIHIAN, H., SARKAR, M., SARGOLZAEI, A., "A novel energy-efficient regenerative braking system for electric vehicles", In: *Proceedings of the SoutheastCon 2024*, pp. 1300–1305, Atlanta, GA, USA, 2024. doi: http://doi.org/10.1109/SoutheastCon52093.2024.10500159.

[25] GUENIAT, F., MARYAM, S., "A comprehensive and policy-oriented model of the hydrogen vehicle fleet composition, applied to the UK market", *Environment Systems & Decisions*, v. 44, n. 1, pp. 85–99, 2024. doi: http://doi.org/10.1007/s10669-023-09911-4.

[26] WALTERMANN, P., "Modelling and control of the longitudinal and lateral dynamics of a series hybrid vehicle", In: *Proceedings of the IEEE International Conference on Control Applications*, pp. 191–198, 1996. doi: http://doi.org/10.1109/CCA.1996.558629.

[27] BAI, H., MI, C., "Power electronics in electric and hybrid vehicles", In: Bai, H., Mi, C. (eds), *Transients of modern power electronics*, Hoboken, John Wiley & Sons,, pp. 71–128, 2011. doi: http://doi.org/10.1002/9781119971719.ch4.

[28] AZMI, M., TOKAI, A., "Electric vehicle and end-of-life vehicle estimation in Malaysia 2040", *Environment Systems & Decisions*, v. 37, n. 4, pp. 451–464, 2017. doi: http://doi.org/10.1007/s10669-017-9647-4.

[29] KIM, M.J., PENG, H., "Power management and design optimization of fuel cell/battery hybrid vehicles", *Journal of Power Sources*, v. 165, n. 2, pp. 819–832, 2007. doi: http://doi.org/10.1016/j.jpowsour.2006.12.038.

[30] XIAO, B., RUAN, J., YANG, W., *et al*., "A review of pivotal energy management strategies for extended range electric vehicles", *Renewable & Sustainable Energy Reviews*, v. 149, pp. 111194, 2021. doi: http://doi.org/10.1016/j.rser.2021.111194.

[31] RANJAN, A., BODKHE, S.B., "Modified energy management strategy for HESS in electric vehicle", In: *Proceedings of the ICPS 2021 - 2021 9th IEEE International Conference on Power Systems (ICPS)*, Kharagpur, India, pp. 1–6, 2021. doi: http://doi.org/10.1109/ICPS52420.2021.9670148.

[32] HATAMI, A., TOUSI, M.R., BAYAT, P., *et al*., "Power management strategy for hybrid vehicle using a three-port bidirectional DC-DC converter", In: *ICEE 2015 - Proceedings of the 23rd Iranian Conference on Electrical Engineering*, Tehran, Iran, pp. 1498–1503, 2015. doi: http://doi.org/10.1109/IranianCEE.2015.7146457.

[33] SNOUSSI, J., BEN ELGHALI, S., BENBOUZID, M., *et al*., "Optimal sizing of energy storage systems using frequency-separation-based energy management for fuel cell hybrid electric vehicles", *IEEE Transactions on Vehicular Technology*, v. 67, n. 10, pp. 9337–9346, 2018. doi: http://doi.org/10.1109/TVT.2018.2863185.

[34] KUMARESAN, N., RAMMOHAN, A., "A comprehensive review on energy management strategies of hybrid energy storage systems for electric vehicles", *Journal of the Brazilian Society of Mechanical Sciences and Engineering*, v. 46, n. 3, pp. 1–25, 2024. doi: http://doi.org/10.1007/s40430-024-04736-x.

[35] AMJADI, Z., WILLIAMSON, S.S., "Power-electronics-based solutions for plug-in hybrid electric vehicle energy storage and management systems", *IEEE Transactions on Industrial Electronics*, v. 57, n. 2, pp. 608–616, 2010. doi: http://doi.org/10.1109/TIE.2009.2032195.

[36] GAN, J., LI, S., LIN, X., *et al*., "Multi-agent deep reinforcement learning-based multi-objective cooperative control strategy for hybrid electric vehicles", *IEEE Transactions on Vehicular Technology*, v. 73, n. 8, pp. 11123–11135, 2024. doi: http://doi.org/10.1109/TVT.2024.3373906.

[37] RAGHUWANSHI, A., OJHA, A., "An overview of the regenerative braking technique and energy storage systems in electric, hybrid, and plug-in hybrid electric vehicles", In: *Proceedings of the IEEE International Students' Conference on Electrical, Electronics and Computer Science (SCEECS)*, Bhopal, India, pp. 1–6, 2023. doi: http://doi.org/10.1109/SCEECS57921.2023.10063062.

[38] NASERI, F., FARJAH, E., GHANBARI, T., "An efficient regenerative braking system based on battery/supercapacitor for electric, hybrid, and plug-in hybrid electric vehicles with BLDC motor", *IEEE Transactions on Vehicular Technology*, v. 66, n. 5, pp. 3724–3738, 2017. doi: http://doi.org/10.1109/TVT.2016.2611655.

[39] DU PASQUIER, A., PLITZ, I., MENOCAL, S., *et al*., "A comparative study of Li-ion battery, supercapacitor and nonaqueous asymmetric hybrid devices for automotive applications", *Journal of Power Sources*, v. 115, n. 1, pp. 171–178, 2003. doi: http://doi.org/10.1016/S0378-7753(02)00718-8.

[40] OPILA, D.F., "Equivalent Degradation Minimization Strategy for balancing battery and capacitor usage in hybrid energy storage systems for electric vehicles", In: *Proceedings of the 2017 American Control Conference (ACC)*, pp. 315–321, 2017. doi: http://doi.org/10.23919/ACC.2017.7962972.

[41] ZHANG, L., HU, X., WANG, Z., *et al*., "Hybrid electrochemical energy storage systems: An overview for smart grid and electrified vehicle applications", *Renewable & Sustainable Energy Reviews*, v. 139, pp. 110581, 2021. doi: http://doi.org/10.1016/j.rser.2020.110581.

[42] NGUYEN, C.T.P., NGUYEN, B.H., TROVAO, J.P.F., *et al*., "Effect of battery/supercapacitor hybrid storage system on battery voltage in electric vehicles", In: *2022 IEEE Vehicle Power and Propulsion Conference (VPPC)*, Merced, CA, USA, 2022. doi: http://doi.org/10.1109/VPPC55846.2022.10003471.

[43] WANG, T., YU, H., ZHU, C., "Hybrid energy sources for hybrid electric vehicle propulsion", In: *2008 IEEE Vehicle Power and Propulsion Conference*, 2008. doi: http://doi.org/10.1109/VPPC.2008.4677787.

[44] SHARF, H.M., ELGHANAM, E.A., HASSAN, M.S., *et al*., "Assessing efficiency and aging of lithium-ion battery in a hybrid energy storage system", In: *2020 IEEE International IOT, Electronics and Mechatronics Conference (IEMTRONICS)*, 2020. doi: http://doi.org/10.1109/IEMTRONICS51293.2020.9216426.

[45] LANG, J., ZHANG, X., LIU, B., *et al*., "The roles of graphene in advanced Li-ion hybrid supercapacitors", *Journal of Energy Chemistry*, v. 27, n. 1, pp. 43–56, 2018. doi: http://doi.org/10.1016/j.jechem.2017.11.020.

[46] AZADMANJIRI, J., SRIVASTAVA, V.K., KUMAR, P., *et al*., "Two- and three-dimensional graphene-based hybrid composites for advanced energy storage and conversion devices", *Journal of Materials Chemistry. A, Materials for Energy and Sustainability*, v. 6, n. 3, pp. 702–734, 2018. doi: http://doi.org/10.1039/C7TA08748A.

[47] XIAO, W., EDWIN, F.F., SPAGNUOLO, G., *et al*., "Efficient approaches for modeling and simulating photovoltaic power systems", *IEEE International Journal of Photovoltaics*, v. 3, n. 1, pp. 500–508, 2013. doi: http://doi.org/10.1109/JPHOTOV.2012.2226435.

[48] TIFIDAT, K., MAOUHOUB, N., "An efficient method for predicting PV modules performance based on the two-diode model and adaptable to the single-diode model", *Renewable Energy*, v. 216, pp. 119102, 2023. doi: http://doi.org/10.1016/j.renene.2023.119102.

[49] THOUNTHONG, P., CHUNKAG, V., SETHAKUL, P., *et al*., "Comparative study of fuel-cell vehicle hybridization with battery or supercapacitor storage device", *IEEE Transactions on Vehicular Technology*, v. 58, n. 8, pp. 3892–3904, 2009. doi: http://doi.org/10.1109/TVT.2009.2028571.

[50] XUN, Q., LIU, Y., HOLMBERG, E., "A comparative study of fuel cell electric vehicles hybridization with battery or supercapacitor", In: *Proceedings of the 2018 International Symposium on Power Electronics, Electrical Drives, Automation and Motion (SPEEDAM)*, pp. 389–394, 2018. doi: http://doi.org/10.1109/SPEEDAM.2018.8445386.

[51] KALAIVANI, P., JOICE, C.S., "Design and modelling of a neural network-based energy management system for solar PV, fuel cell, battery and ultracapacitor-based hybrid electric vehicle", *Electrical Engineering*, v. 106, n. 1, pp. 689–709, 2024. doi: http://doi.org/10.1007/s00202-023-02015-x.

[52] MAARUF, M., EL-FERIK, S., "Neural learning fault-tolerant control of fuel cell–battery–ultracapacitor-based hybrid electric vehicle", *Journal of Energy Storage*, v. 98, pp. 112892, 2024. doi: http://doi.org/10.1016/j.est.2024.112892.

[53] BURKE, A.F., "Batteries and ultracapacitors for electric, hybrid, and fuel cell vehicles", *Proceedings of the IEEE*, v. 95, n. 4, pp. 806–820, 2007. doi: http://doi.org/10.1109/JPROC.2007.892490.

[54] JONDHLE, H., NANDGAONKAR, A.B., NALBALWAR, S., *et al*., "An artificial intelligence and improved optimization-based energy management system of battery-fuel cell-ultracapacitor in hybrid electric vehicles", *Journal of Energy Storage*, v. 74, pp. 109079, 2023. doi: http://doi.org/10.1016/j.est.2023.109079.

[55] KHALIGH, A., LI, Z., "Battery, ultracapacitor, fuel cell, and hybrid energy storage systems for electric, hybrid electric, fuel cell, and plug-in hybrid electric vehicles: state of the art", *IEEE Transactions on Vehicular Technology*, v. 59, n. 6, pp. 2806–2814, 2010. doi: http://doi.org/10.1109/TVT.2010.2047877.

[56] KHAN, F.A., MEKHILEF, S., RAMACHANDARAMURTHY, V.K., *et al*., "Design and development of grid independent integrated energy system for electric vehicle charging stations at different locations in Malaysia", *Energy*, v. 302, pp. 131686, 2024. doi: http://doi.org/10.1016/j.energy.2024.131686.

[57] RADE, M.R., "Design and Development of Hybrid Energy Storage System for Electric Vehicle", In: *Proceedings of the International Conference on Information, Communication, Engineering and Technology (ICICET)*, pp. 1–5, 2018. doi: http://doi.org/10.1109/ICICET.2018.8533757.

[58] CHEMALI, E., PREINDL, M., MALYSZ, P., *et al*., "Electrochemical and electrostatic energy storage and management systems for electric drive vehicles: state-of-the-art review and future trends", *IEEE Journal of Emerging and Selected Topics in Power Electronics*, v. 4, n. 3, pp. 1117–1134, 2016. doi: http://doi.org/10.1109/JESTPE.2016.2566583.

[59] ZHANG, J.W., WANG, Y.H., LIU, G.C., *et al*., "A review of control strategies for flywheel energy storage system and a case study with matrix converter", *Energy Reports*, v. 8, pp. 3948–3963, 2022. doi: http://doi.org/10.1016/j.egyr.2022.03.009.

[60] LIM, W.C., TEO, B.C.T., LIM, X.Y., *et al*., "Comparative analysis of passive, active, and hybrid cell balancing for optimal battery performance", In: *Proceedings of the 2024 International Conference on Electronics, Information, and Communication (ICEIC)*, pp. 1–4, 2024. doi: http://doi.org/10.1109/ICEIC61013.2024.10457118.

[61] RAEBER, M., HEINZELMANN, A., ABDESLAM, D.O., "Analysis of an active charge balancing method based on a single nonisolated DC/DC converter", *IEEE Transactions on Industrial Electronics*, v. 68, n. 3, pp. 2257–2265, 2021. doi: http://doi.org/10.1109/TIE.2020.2972449.

[62] KARTHIK, K., PONNAMBALAM, P., "Analysis of cell balancing of Li-ion batteries with dissipative and non-dissipative systems for electric vehicle applications", *Energy Reports*, v. 12, pp. 2408–2428, 2024. doi: http://doi.org/10.1016/j.egyr.2024.08.023.

[63] APHALE, S., KELANI, A., NANDURDIKAR, V., *et al*., "Li-ion batteries for electric vehicles: Requirements, state of art, challenges and future perspectives", In: *Proceedings of the IEEE International Conference on Power and Energy (PECon)*, pp. 288–292, 2020. doi: http://doi.org/10.1109/PECon48942.2020.9314515.

[64] DURAISAMY, T., KALIYAPERUMAL, D., "Machine learning-based optimal cell balancing mechanism for electric vehicle battery management system", *IEEE Access: Practical Innovations, Open Solutions*, v. 9, pp. 132846–132861, 2021. doi: http://doi.org/10.1109/ACCESS.2021.3115255.

[65] PATEL, J., CHANDWANI, H., PATEL, V., *et al*., "Bi-directional DC-DC converter for battery charging: discharging applications using buck-boost switch", In: *Proceedings of the IEEE Students' Conference on Electrical, Electronics and Computer Science*, v. 1–4, pp. 1–4, 2012. doi: http://doi.org/10.1109/SCEECS.2012.6184993.

[66] ELSAYAD, N., MORADISIZKOOHI, H., MOHAMMED, O., "A new SEPIC-based step-up DC-DC converter with wide conversion ratio for fuel cell vehicles: analysis and design", *IEEE Transactions on Industrial Electronics*, v. 68, n. 8, pp. 6390–6400, 2021. doi: http://doi.org/10.1109/TIE.2020.3007110.

[67] AGUILAR LOPEZ, F., BILLY, R.G., MÜLLER, D.B., *et al*., "Analysis of li-ion battery characteristics in a wearable patient monitoring device using equivalent circuit model", In: *Proceedings of the IEEE International Conference on Power and Energy (PECon 2020)*, pp. 288–292, 2020. doi: http://doi.org/10.1016/j.resconrec.2023.106951.